

Measurement-induced integer families of critical dynamical scaling in quantum many-body systems

Zuo Wang,^{1,2} Shi-Liang Zhu,^{1,2,*} Li-Jun Lang,^{1,2,†} and Liang He^{1,2,‡}

¹Key Laboratory of Atomic and Subatomic Structure and Quantum Control (Ministry of Education), School of Physics, South China Normal University, Guangzhou 510006, China

²Guangdong Provincial Key Laboratory of Quantum Engineering and Quantum Materials, Guangdong-Hong Kong Joint Laboratory of Quantum Matter, South China Normal University, Guangzhou 510006, China

A quantum many-body system can undergo transitions in the presence of continuous measurement. In this work, we find that a generic class of critical dynamical scaling behavior can emerge at these measurement-induced transitions. Remarkably, depending on the symmetry that can be respected by the system, different integer families of dynamical scaling can emerge. The origin of these scaling families can be traced back to the presence of hierarchies of high order exceptional points in the effective non-Hermitian descriptions of the systems. Direct experimental observation of this class of dynamical scaling behavior can be readily achieved using ultracold atoms in optical lattices or through intermediate-scale quantum computing systems.

Introduction.—Quantum technology has undergone rapid development in recent decades [1]. Particularly, in the field of quantum information science, both digital quantum computers, represented by quantum circuits [2–5], and analog quantum computers, represented by programmable quantum simulators [6–10], have achieved high levels of controllability. Quantum measurements play a crucial role in extracting useful information from these devices, and in certain cases, they can also be utilized to prepare nontrivial quantum states, such as random states that are essential for quantum information applications [11]. Recently, these technological advancements have also motivated investigations into a fundamental class of questions, broadly categorized as measurement-induced transitions in quantum many-body systems. These investigations encompass transitions induced by different types of measurement protocols, including continuous measurements [12–14], random projective selections [14–18], measurements with post-selection [19–22]. Notably, non-trivial dynamical scaling behavior of entanglement has been identified in various scenarios [12–29].

Viewing measurements as influences imposed by the environment, quantum systems under measurement fall into the category of open quantum systems [30, 31]. These systems exhibit key features such as possible breaking of detailed balance, making them inherently non-equilibrium. From this perspective, measurement-induced transitions can be classified as non-equilibrium transitions, which can exhibit much richer dynamical scaling behavior compared to equilibrium transitions. For instance, the well-known dynamical behavior described by the Kardar-Parisi-Zhang equations is not only found in typical growing interface dynamics [32] but also observed in various quantum systems such as exciton-polariton condensates [33, 34]. Remarkably, certain families of dynamical scaling can emerge in non-equilibrium systems, such as the Fibonacci family of dynamical scal-

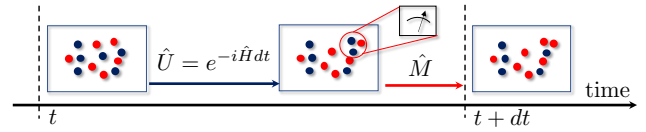


Figure 1. Schematic illustration of the quantum many-body dynamics in the presence of continuous measurements. In each short time interval dt , the system undergoes a unitary evolution $\hat{U} = e^{-i\hat{H}dt}$ governed by its Hamiltonian \hat{H} . Subsequently, a local or global measurement \hat{M} is conducted on the system, and the quantum trajectories are post-selected based on the measurement outcome.

ing found in the multi-component asymmetric simple exclusion process [35]. In this context, a fundamental question arises regarding the existence of non-trivial critical dynamical scaling in physical observables and their properties beyond the entanglement of the systems.

In this work, we address this question for several quantum many-body systems under continuous measurements and find that a generic class of dynamical scaling indeed emerges at these measurement-induced transitions. Remarkably, different integer families of dynamical scaling (IFDS) can emerge depending on the symmetry that can be respected by the system. These scalings are distinct from the scaling of conventional phase transitions as they can emerge even in finite-sized systems without requiring the thermodynamic limit. The origin of these scaling families can be attributed to the hierarchies of exceptional points (EPs) present in the effective non-Hermitian descriptions of the systems. Experimental observation of this class of dynamical scaling can be readily performed in various current experimental setups.

Measurement protocol and measurement-induced dynamical scaling in the transverse Ising model.—The type of the measurement protocol considered here pertains to a continuous monitoring or variable strength weak measurements [36]. For a generic quantum many-body

system, its dynamics within each short time interval dt is governed by its Hamiltonian \hat{H} and an operator \hat{M} that encapsulates the measurement effect on the system. The evolution of the quantum state $|\psi(t)\rangle$ is given by $|\psi(t+dt)\rangle = \hat{M}e^{-i\hat{H}dt}|\psi(t)\rangle$ (units $\hbar = 1$) as illustrated schematically in Fig. 1.

Let us begin by considering the transverse Ising model under monitoring (the periodic boundary is assumed). Previous studies have demonstrated that this model, under global monitoring, exhibits a measurement-induced transition [37]. Here, we explore a more general scenario where the transverse field is local, and the measurement is also performed on the region of the local transverse field. The system's dynamics is determined by the Hamiltonian \hat{H}_{TI} and the measurement operator \hat{M}_{S} , where

$$\hat{H}_{\text{TI}} = -J \sum_{j=1}^L \hat{\sigma}_j^z \hat{\sigma}_{j+1}^z - g \sum_{j \in \mathcal{M}} \hat{\sigma}_j^x, \quad (1)$$

$$\hat{M}_{\text{S}} = 1 - \gamma dt \sum_{j \in \mathcal{M}} (1 - \hat{\sigma}_j^y). \quad (2)$$

Here, $\hat{\sigma}_j^x$, $\hat{\sigma}_j^y$, $\hat{\sigma}_j^z$ represent the three Pauli operators on site j , J denotes the strength of the ferromagnetic coupling, g represents the strength of the local transverse field along the x -direction, and \mathcal{M} denotes both region of measurement and local transverse field. The measurement effect on the system is encapsulated in the operator \hat{M}_{S} . Specifically, it corresponds to performing a weak measurement on the spin-down state along the y -direction with a strength characterized by γ , and post-selecting the trajectories where the spin-down state along the y -direction is not detected [37] (see Supplemental Material (SM) [38]).

Prior investigations have shown that when the measurement strength γ matches the strength of the transverse field g , the entanglement of the system undergoes a sharp transition and exhibits critical behavior [37]. Now, we examine whether such criticality is also manifested in other experimentally accessible observables.

To this end, we numerically simulate the dynamics according to $|\psi(t+dt)\rangle = \hat{M}_{\text{S}}e^{-i\hat{H}_{\text{TI}}dt}|\psi(t)\rangle$ and calculate the time dependence of the total magnetization along the z -direction $|S_z(t)| \equiv |\langle \Psi(t) | \sum_{j=1}^L \hat{\sigma}_j^z / 2 | \Psi(t) \rangle|$ in the “renormalized” state $|\Psi(t)\rangle \equiv e^{|\mathcal{M}|\gamma t} |\psi(t)\rangle$ with $|\mathcal{M}|$ being the cardinality of \mathcal{M} . The pre-factor $e^{|\mathcal{M}|\gamma t}$ introduced in $|\Psi(t)\rangle$ is intended to eliminate the trivial exponential decay of the module of $|\psi(t)\rangle$ caused by the post-selection of trajectories. Fig. 2(a1) illustrates the time evolution of $|S_z(t)|$ for a system with $L = 5$ and $|\mathcal{M}| = 1$ at different measurement strengths γ . Notably, as γ approaches g , $|S_z(t)|$ manifests a scaling behavior of $|S_z(t)| \propto t^2$ in the “late time” dynamics.

To quantitatively analyze the emergence of this scaling, we determine a characteristic timescale τ by performing fits of a simple exponential function $Ae^{t/\tau}$ and an oscillatory

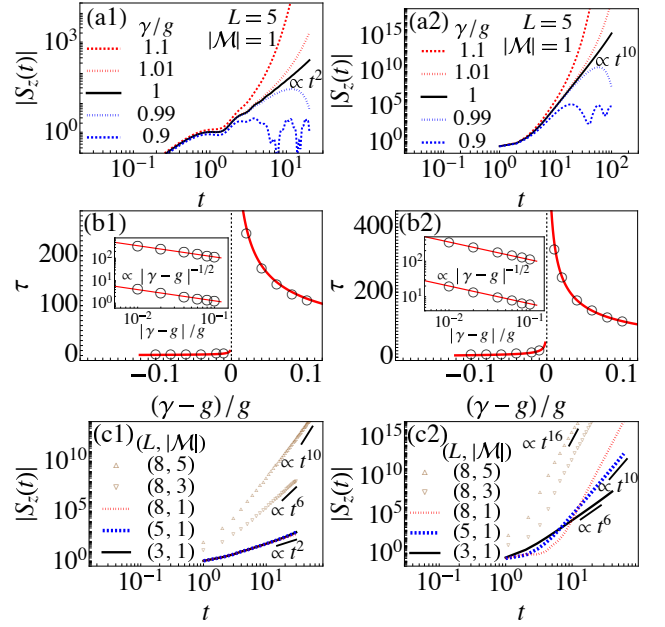


Figure 2. Quantum dynamics of the transverse Ising (a1, b1, c1) and Heisenberg (a2, b2, c2) model under monitoring. (a1, a2) Time dependence of $|S_z(t)|$ at different γ/g values. Power law scaling $|S_z(t)| \propto t^2$ emerges as $\gamma/g \rightarrow 1$. (b1, b2) Characteristic time τ manifests a power divergence $\tau \propto |\gamma - g|^{-1/2}$ for $\gamma/g \rightarrow 1$. (c1, c2) Power law scaling of $|S_z(t)|$ at critical point $\gamma/g = 1$ for different system and measurement region sizes. Transverse Ising model manifests an IFDS $|S_z(t)| \propto t^{2|\mathcal{M}|}$ (c1), while transverse Heisenberg model manifests an IFDS $|S_z(t)| \propto t^{2L}$ (c2). All dynamics are simulated with $J = 1$, $g = 1$, $dt = 10^{-4}$, $\mathcal{M} = \{1, 2, \dots, |\mathcal{M}|\}$, and the initial state give by $|\psi(t=0)\rangle = 2^{-L} \sum_{\{\sigma_i\}} |\sigma_1 \sigma_2 \dots \sigma_L\rangle$.

latory function $B \cos(t/\tau + \theta) + C$ (A , B , C , θ and τ are real fitting parameters) to the numerical data of $|S_z(t)|$ for $\gamma/g > 1$ and $\gamma/g < 1$, respectively. As shown in Fig. 2(b1), the emergence of the dynamical scaling coincides with the divergence of the characteristic timescale τ , reminiscent of the similar behavior in traditional continuous phase transitions. Interestingly, we observe a power law scaling of τ with respect to the distance between the measurement strength γ to its critical value $\gamma = g$, i.e., $\tau \propto |\gamma - g|^{-1/2}$. Furthermore, for this single-site measurement case ($|\mathcal{M}| = 1$), we calculate $|S_z(t)|$ at the transition point $g = \gamma$ at different system sizes with $L = 3, 5, 8$. As shown by the lower three curves in Fig. 2(c1), we observe that $|S_z(t)|$ manifests the same dynamical scaling $\propto t^2$ in the “late time” dynamics. These results clearly demonstrate that, beyond the entanglement entropy, other physical observables can indeed exhibit critical scaling at the transition point.

IFDS in transverse Heisenberg and Ising spin chain under monitoring.—The scaling behavior at the critical point of a system is known to be strongly influenced by its underlying symmetry. Hence, it is of great interest to explore systems that exhibit different symmetries. Mo-

tivated by this, we investigate the behavior of a local transverse field ferromagnetic spin-1/2 Heisenberg chain under monitoring, considering a periodic boundary condition. The dynamics of this system are governed by the Hamiltonian

$$\hat{H}_{\text{TH}} = -J \sum_{j=1}^L \sum_{a=x,y,z} \hat{\sigma}_j^a \hat{\sigma}_{j+1}^a - g \sum_{j \in \mathcal{M}} \hat{\sigma}_j^x, \quad (3)$$

along with the measurement operator \hat{M}_{S} defined in Eq. (2). Fig. 2(a2) illustrates the time evolution of $|S_z(t)|$ for the system with $L = 5$, $|\mathcal{M}| = 1$ at various measurement strength γ . Similar to the transverse Ising model, as γ approaches g , $|S_z(t)|$ manifests scaling behavior characterized by $|S_z(t)| \propto t^\alpha$ in its late-time dynamics. However, in contrast to the Ising case, the scaling exponent assumes a surprisingly larger value of $\alpha = 10$, even though the characteristic timescale τ exhibits the same diverging behavior, i.e., $\tau \propto |\gamma - g|^{-1/2}$ [Fig. 2(b2)].

To validate the value of the scaling exponent, we further examine time dependence of $|S_z(t)|$ at the critical point for different system sizes. However, we observe a strong dependence of the dynamical scaling of $|S_z(t)|$ on the system size L , as shown in Fig. 2(c2). At first glance, this may seem to be a manifestation of the finite size effects. However, upon closer inspection of the scaling exponent α for different system sizes, we find that they all take sharp integer values. In fact, from the results presented in Fig. 2(c2), one can deduce a simple empirical formula $\alpha = 2L$ for the exponents corresponding to different system sizes. Calculations involving more system sizes (see SM [38]) further confirm the validity of this empirical formula.

Interestingly, for the transverse Ising chain under monitoring [see Eqs. (1, 2)], although the scaling exponent does not change with respect to the system size L , it actually manifest a dependence on the size of the measurement region $|\mathcal{M}|$. As shown by the upper curves in Fig. 2(c1) which correspond to different $|\mathcal{M}|$, we observe that the exponent can be empirically described by a simple formula $\alpha = 2|\mathcal{M}|$. Further calculations involving additional measurement sizes (see SM [38]) support the validity of this empirical formula.

The numerical results presented above strongly indicate that these two systems can exhibit distinct IFDS, with their exponents being determined either by the system size in the Heisenberg case or by the size of the measurement region in the Ising case. Moreover, these findings suggest that the emergence of these IFDS cannot be merely coincidental. Indeed, as we shall show in the following, the emergence of these IFDS can be attributed to the presence of series of high-order EPs in the non-Hermitian effective descriptions of these systems.

Non-Hermitian effective descriptions.—In the limit of continuous measurement ($\gamma dt \ll 1$), it is possible to construct an effective non-Hermitian Hamiltonian [20–22]

that faithfully captures (up to Trotter error) the system's physics [38]. For the transverse Ising chain under monitoring [Eqs. (1, 2)], the measurement \hat{M}_{S} can be well approximated by $e^{-\gamma dt \sum_{j \in \mathcal{M}} (1 - \hat{\sigma}_j^y)}$ in this limit. This allows us to effectively capture the system's time evolution through the introduction of a non-Hermitian effective Hamiltonian, denoted as $\hat{H}_{\text{TI}}^{\text{eff}} = -J \sum_{j=1}^L \hat{\sigma}_j^z \hat{\sigma}_{j+1}^z - \sum_{j \in \mathcal{M}} [g \hat{\sigma}_j^x + i\gamma(1 - \hat{\sigma}_j^y)]$. Notably, the non-Hermitian term, $-i \sum_{j \in \mathcal{M}} \gamma(1 - \hat{\sigma}_j^y)$ adequately incorporates the physical consequences of the measurements. Similar construction can be carried out for the Heisenberg spin-chain [Eq. (3)] under monitoring, leading to a non-Hermitian effective Hamiltonian $\hat{H}_{\text{TH}}^{\text{eff}} = -J \sum_{j=1}^L \sum_{a=x,y,z} \hat{\sigma}_j^a \hat{\sigma}_{j+1}^a - \sum_{j \in \mathcal{M}} [g \hat{\sigma}_j^x + i\gamma(1 - \hat{\sigma}_j^y)]$.

We notice from Fig. 2 that both for the Ising and the Heisenberg cases, the onset of dynamical scaling behavior is observed precisely at the parameter point $g = \gamma$. Remarkably, this parameter point corresponds to the one at which the EPs emerge in the local competition term between the transverse field and the measurement, i.e., $g \hat{\sigma}_j^x + i\gamma(1 - \hat{\sigma}_j^y)$ in the non-Hermitian effective Hamiltonians $\hat{H}_{\text{TI}}^{\text{eff}}$ and $\hat{H}_{\text{TH}}^{\text{eff}}$. While it is generally not guaranteed for a non-Hermitian Hamiltonian that the EP of its constituent parts aligns with its own EP, we find that this is indeed the case in this scenario (see SM [38] for mathematical proof). This intriguing outcome can be attributed to the symmetry associated with the domain-wall conservation preserved by $\hat{H}_{\text{TI}}^{\text{eff}}$ and the SU(2) symmetry respected by $\hat{H}_{\text{TH}}^{\text{eff}}$ at $g = \gamma = 0$ (see SM [38]). Specifically, in the Ising case with $|\mathcal{M}| \leq L - 2$, we find that EPs of different orders appear for $\hat{H}_{\text{TI}}^{\text{eff}}$ at $g = \gamma$, with the highest order being $|\mathcal{M}| + 1$. While in the Heisenberg case, regardless of the size of the measurement region $|\mathcal{M}|$, EPs of different orders appear for $\hat{H}_{\text{TH}}^{\text{eff}}$ at $g = \gamma$, with the highest order being $L + 1$. As we shall see in the following, it is precisely these EPs of the highest order that gives rise to the observed IFDS in the transverse Heisenberg and Ising chain, as shown in Figs. 2(c1, c2).

According to the general theory regarding the Jordan form [39], for a generic non-Hermitian Hamiltonian $\hat{\mathcal{H}}$, some of the eigenvectors belonging to the same eigenvalue coalesce at EPs. Consequentially, in order to find a complete basis spanning the entire Hilbert space, one can use the set of so-called generalized eigenvectors $\{|V_n^{(j)}\rangle\}$ [39], where $|V_n^{(j)}\rangle$ denotes the n th generalized eigenvector that corresponds to the j th Jordan block with the eigenvalue λ_j . With this complete basis $\{|V_n^{(j)}\rangle\}$, any generic state $|\psi\rangle$ can be expanded as $|\psi\rangle = \sum_{j=1}^{N_{\text{JB}}} \sum_{n=1}^{\mathcal{O}_j} c_n^{(j)} |V_n^{(j)}\rangle$, where $c_n^{(j)}$ are the expansion coefficients, N_{JB} is the number of Jordan blocks of $\hat{\mathcal{H}}$, \mathcal{O}_j is the order of the j th Jordan block (for $\mathcal{O}_j \geq 2$, \mathcal{O}_j is the order of the corresponding EP). Notably, the time evolution of generalized eigenvec-

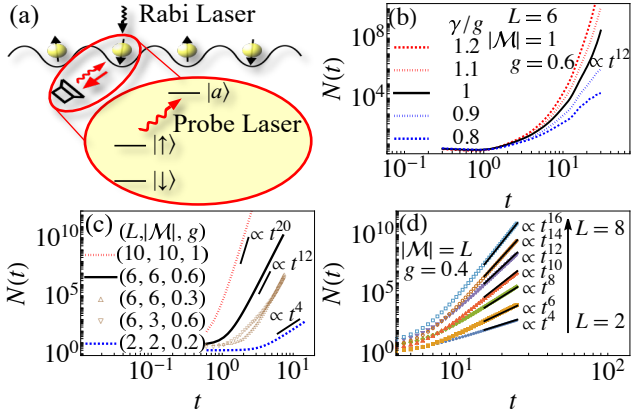


Figure 3. Quantum dynamics of Fermi gases in optical lattices under monitoring. (a) Schematic illustration of Fermi gases in optical lattices and the implementation of measurements. (b) Time dependence of $N(t)$ at different γ/g for $L = 6$. Power law scaling $N(t) \propto t^{12}$ emerges as $\gamma/g \rightarrow 1$. (c) Scalings of $N(t)$ at the critical point $\gamma/g = 1$ for different $(L, |\mathcal{M}|, g)$. (d) IFDS $N(t) \propto t^{2L}$ at the critical point $\gamma/g = 1$. The simulations are performed with $J = 1$, $U = 5$, $dt = 10^{-3}$, and the initial state given by $|\psi(t=0)\rangle = |\uparrow_1, \dots, \uparrow_{L/2}, \downarrow_{L/2+1}, \dots, \downarrow_L\rangle$, with measurements conducted in the central region of the system.

tors assumes the form [38, 40]

$$e^{-i\hat{H}t} |V_n^{(j)}\rangle = e^{-i\lambda_j t} \sum_{m=0}^{n-1} \frac{(-it)^m}{m!} |V_{n-m}^{(j)}\rangle. \quad (4)$$

From Eq. (4), it becomes apparent that in the late-time regime ($t \gg 1$), the dominant term in $|\psi(t)\rangle$ is $e^{-i\lambda_{j_{\max}} t} (-it)^{\mathcal{O}_{j_{\max}}-1} [(\mathcal{O}_{j_{\max}} - 1)!]^{-1} |V_1^{(j_{\max})}\rangle$, where $\mathcal{O}_{j_{\max}} = \max\{\mathcal{O}_j\}$. This indicates that the expectation value of generic observables $\langle \hat{O} \rangle(t) \equiv \langle \psi(t) | \hat{O} | \psi(t) \rangle$ should exhibit the dynamical scaling $\propto t^{2(\mathcal{O}_{j_{\max}}-1)}$ in the late-time dynamics provided $\langle V_1^{(j_{\max})} | \hat{O} | V_1^{(j_{\max})} \rangle \neq 0$ [41]. As we have seen earlier, for $\hat{H}_{\text{TH}}^{\text{eff}}$ at $g = \gamma$, the EP with the highest order is of order $L + 1$, i.e., $\mathcal{O}_{j_{\max}} = L + 1$, and the EP with the highest order is of order $|\mathcal{M}| + 1$ for $\hat{H}_{\text{TI}}^{\text{eff}}$ at $g = \gamma$. Consequently, in the late-time regime of the Heisenberg and Ising case, the expectation value of generic observables, such as $\langle S_z(t) \rangle$, is expected to exhibit dynamical scaling behavior of $\propto t^{2L}$ and $\propto t^{2|\mathcal{M}|}$, respectively. This precisely corresponds to the observed IFDS in the transverse Heisenberg and Ising chain under monitoring [see Figs. 2(c1, c2)]. Furthermore, the power law divergence of the characteristic timescales τ at the measurement induced transition [see Figs. 2(b1, b2)] can also be attributed to the dynamical behavior in the vicinity of the EPs associated with the parity-time reversal symmetry breaking of the systems' non-Hermitian effective descriptions (see SM [38]).

IFDS in optical lattices.—The preceding discussion has focused on spin systems and we notice that the essential structure that leads to the emergence of the IFDS is the

symmetry that can be assumed in the system. This motivates us to investigate the IFDS beyond spin systems. One case in point is ultracold Fermi gases in optical lattices, which not only respects the same SU(2) symmetry as the Heisenberg spin chain, but is also highly pertinent to experiments with ultracold atoms [42–45].

As illustrated schematically in Fig. 3(a), the system being monitored is an ultracold spin-1/2 Fermi gas loaded in a 1D optical lattice, a part of which is shined by a Rabi laser that couples the two internal states of the atoms. An observer repeatedly perform “weak” measurements on the occupation of spin-up atoms in the shined region and decide whether the system continue evolving according to the measurement outcome.

More specifically, the Hamiltonian of the system reads

$$\hat{H}_F = -J \sum_{j=1}^{L-1} \sum_{\sigma} (\hat{c}_{j,\sigma}^{\dagger} \hat{c}_{j+1,\sigma} + \text{h. c.}) + U \sum_{j=1}^L \hat{n}_{j,\uparrow} \hat{n}_{j,\downarrow} \quad (5) \\ + g \sum_{j \in \mathcal{M}} (\hat{c}_{j,\uparrow}^{\dagger} \hat{c}_{j,\downarrow} + \hat{c}_{j,\downarrow}^{\dagger} \hat{c}_{j,\uparrow}),$$

where $\hat{c}_{j,\sigma}^{\dagger}$ ($\hat{c}_{j,\sigma}$) is the creation (annihilation) operator of the fermions with spin σ ($\sigma = \uparrow, \downarrow$) at the j th site and $\hat{n}_{j,\sigma} \equiv \hat{c}_{j,\sigma}^{\dagger} \hat{c}_{j,\sigma}$ is the particle number operator counting the number of atoms with spin σ on site j . The first two terms in (5) are the conventional hopping term and the on-site interaction term, with their strengths being J and U , respectively. The third term is a spin flip term that describes the coupling between the Rabi laser and the atoms within the region specified by \mathcal{M} , with its strength being g . From the form of Hamiltonian (5), one can see that this system can be readily realized in current ultracold atom experiments employing ultracold Fermi gases in optical lattices.

The measurement imposed on the system is described by the operator $\hat{M}_F = 1 - dt\gamma \sum_{j \in \mathcal{M}} (\hat{n}_{j,\uparrow} - \hat{n}_{j,\downarrow})$ [38] with γ characterizing the strength of the measurement. For Fermi gases in deep optical lattices at half filling, this corresponds to weakly measuring the occupation of spin-up atoms in the region \mathcal{M} , followed by post-selection of the quantum trajectories without spin-up atoms. Specifically, as schematically illustrated in Fig. 3(a), this measurement process can be implemented in experiments by weakly coupling the internal $|\uparrow\rangle$ state of the atoms to an auxiliary state $|a\rangle$ with a probe laser and subsequently performing postselection based on the results of the strong measurements with respect to $|a\rangle$ [38, 46].

Fig. 3(b) presents the time evolution of the total particle number $N(t) \equiv \langle \psi(t) | \sum_{j,\sigma} \hat{n}_{j,\sigma} | \psi(t) \rangle$ at different measurement strengths for $L = 6$, starting from an easily accessible initial state in experiments, namely, $|\psi(0)\rangle = |\uparrow_1, \dots, \uparrow_{L/2}, \downarrow_{L/2+1}, \dots, \downarrow_L\rangle$. Notably, as the measurement strength γ approaches the Rabi coupling strength g , $N(t)$ exhibits a clear dynamical scaling $\propto t^{12}$. To explore the possible IFDS of the system, we further calculate $N(t)$ of the systems at different $(L, |\mathcal{M}|, g)$ as shown

in Figs. 3(c, d). From these results, one notices that an IFDS, $N(t) \propto t^{2L}$, indeed exists for the system, regardless of the size of the region under monitoring. This clearly suggests the robustness of the observed IFDS, making them readily accessible for experimental observation. In particular, for current ultracold atom experiments in the deep optical lattices and half-filling regime, the measurement protocol can be relatively easily implemented as discussed above (see SM [38] for more general cases without deep optical lattices and more details on the experimental observability).

Conclusion and discussion.—We have revealed that IFDS can emerge in quantum many-body systems under monitoring, with the scaling exponents determined by the order of the hierarchy of EPs present in the system's effective non-Hermitian description. Although our investigation has focused on 1D systems, it is noteworthy that IFDS can also exist in high-dimensional Heisenberg spin systems and Fermi gases in optical lattices as the key mechanism underlying this IFDS is the internal SU(2) symmetry. Moreover, the thermodynamic limit is not mandatory for the manifestation of these distinctive dynamical scaling behavior, greatly facilitating the direct experimental observation of IFDS across a plethora of platforms, such as ultracold atoms in optical lattices [42–45, 47–49], the trapped-ion [50] or superconducting quantum computing systems [6]. Our predictions will also stimulate further research on the critical scaling in measurement induced transitions, encompassing diverse measurement protocols like random projective selections.

We thank Guo-Qing Zhang and Zheng-Yuan Xue for helpful discussions. This work was supported by NKRDPC (Grant Nos. 2022YFA1405300), NSFC (Grant Nos. 12074180, and 12275089), Guangdong Basic and Applied Research Foundation (Grant No. 2023A1515012800), Guangdong Provincial Key Laboratory (Grant No. 2020B1212060066), Key-Area Research and Development Program of Guangdong Province (Grant No. 2019B030330001), and START grant of South China Normal University.

* slzhu@scnu.edu.cn

† ljlang@scnu.edu.cn

‡ liang.he@scnu.edu.cn

- [1] J. Preskill, *Quantum* **2**, 79 (2018).
- [2] S. Lloyd, *Science* **273**, 1073 (1996).
- [3] F. Arute, K. Arya, R. Babbush, D. Bacon, J. C. Bardin, R. Barends, R. Biswas, S. Boixo, F. G. Brandao, D. A. Buell, *et al.*, *Nature* **574**, 505 (2019).
- [4] H.-S. Zhong, H. Wang, Y.-H. Deng, M.-C. Chen, L.-C. Peng, Y.-H. Luo, J. Qin, D. Wu, X. Ding, Y. Hu, *et al.*, *Science* **370**, 1460 (2020).
- [5] Y. Wu, W.-S. Bao, S. Cao, F. Chen, M.-C. Chen, X. Chen, T.-H. Chung, H. Deng, Y. Du, D. Fan, *et al.*, *Phys. Rev. Lett.* **127**, 180501 (2021).
- [6] I. M. Georgescu, S. Ashhab, and F. Nori, *Rev. Mod. Phys.* **86**, 153 (2014).
- [7] H. Bernien, S. Schwartz, A. Keesling, H. Levine, A. Omran, H. Pichler, S. Choi, A. S. Zibrov, M. Endres, M. Greiner, V. Vuletić, and M. D. Lukin, *Nature* **551**, 579 (2017).
- [8] A. Browaeys and T. Lahaye, *Nat. Phys.* **16**, 132 (2020).
- [9] G. Semeghini, H. Levine, A. Keesling, S. Ebadi, T. T. Wang, D. Bluvstein, R. Verresen, H. Pichler, M. Kalinowski, R. Samajdar, A. Omran, S. Sachdev, A. Vishwanath, M. Greiner, V. Vuletić, and M. D. Lukin, *Science* **374**, 1242 (2021).
- [10] G. Giudici, M. D. Lukin, and H. Pichler, *Phys. Rev. Lett.* **129**, 090401 (2022).
- [11] J. Choi, A. L. Shaw, I. S. Madjarov, X. Xie, R. Finkelstein, J. P. Covey, J. S. Cotler, D. K. Mark, H.-Y. Huang, A. Kale, H. Pichler, F. G. S. L. Brandão, S. Choi, and M. Endres, *Nature* **613**, 468 (2023).
- [12] M. J. Gullans and D. A. Huse, *Phys. Rev. X* **10**, 041020 (2020).
- [13] S.-K. Jian, C. Liu, X. Chen, B. Swingle, and P. Zhang, *Phys. Rev. Lett.* **127**, 140601 (2021).
- [14] Y. Fuji and Y. Ashida, *Phys. Rev. B* **102**, 054302 (2020).
- [15] B. Skinner, J. Ruhman, and A. Nahum, *Phys. Rev. X* **9**, 031009 (2019).
- [16] Y. Li, X. Chen, and M. P. A. Fisher, *Phys. Rev. B* **98**, 205136 (2018).
- [17] Y. Li, X. Chen, and M. P. A. Fisher, *Phys. Rev. B* **100**, 134306 (2019).
- [18] R. Fan, S. Vijay, A. Vishwanath, and Y.-Z. You, *Phys. Rev. B* **103**, 174309 (2021).
- [19] A. Nahum, S. Roy, B. Skinner, and J. Ruhman, *PRX Quantum* **2**, 010352 (2021).
- [20] S. Gopalakrishnan and M. J. Gullans, *Phys. Rev. Lett.* **126**, 170503 (2021).
- [21] S.-K. Jian, Z.-C. Yang, Z. Bi, and X. Chen, *Phys. Rev. B* **104**, L161107 (2021).
- [22] X. Turkeshi, A. Biella, R. Fazio, M. Dalmonte, and M. Schiró, *Phys. Rev. B* **103**, 224210 (2021).
- [23] A. Chan, R. M. Nandkishore, M. Pretko, and G. Smith, *Phys. Rev. B* **99**, 224307 (2019).
- [24] S. Choi, Y. Bao, X.-L. Qi, and E. Altman, *Phys. Rev. Lett.* **125**, 030505 (2020).
- [25] S. Goto and I. Danshita, *Phys. Rev. A* **102**, 033316 (2020).
- [26] C.-M. Jian, Y.-Z. You, R. Vasseur, and A. W. W. Ludwig, *Phys. Rev. B* **101**, 104302 (2020).
- [27] M. J. Gullans and D. A. Huse, *Phys. Rev. Lett.* **125**, 070606 (2020).
- [28] S. Sang and T. H. Hsieh, *Phys. Rev. Res.* **3**, 023200 (2021).
- [29] C. Noel, P. Niroula, D. Zhu, A. Risinger, L. Egan, D. Biswas, M. Cetina, A. V. Gorshkov, M. J. Gullans, D. A. Huse, and C. Monroe, *Nat. Phys.* **18**, 760 (2022).
- [30] C. W. Gardiner and P. Zoller, *Quantum Noise* (Springer, Berlin, 2000).
- [31] H. P. Breuer and F. Petruccione, *The Theory of Open Quantum Systems* (Oxford University Press, 2002).
- [32] M. Kardar, G. Parisi, and Y.-C. Zhang, *Phys. Rev. Lett.* **56**, 889 (1986).
- [33] K. Deligiannis, Q. Fontaine, D. Squizzato, M. Richard, S. Ravets, J. Bloch, A. Minguzzi, and L. Canet, *Phys. Rev. Res.* **4**, 043207 (2022).
- [34] Q. Fontaine, D. Squizzato, F. Baboux, I. Amelio,

- A. Lemaître, M. Morassi, I. Sagnes, L. Le Gratiet, A. Harouri, M. Wouters, *et al.*, *Nature* **608**, 687 (2022).
- [35] V. Popkov, A. Schadschneider, J. Schmidt, and G. M. Schütz, *Proceedings of the National Academy of Sciences* **112**, 12645 (2015).
- [36] D. A. Ivanov, T. Y. Ivanova, S. F. Caballero-Benitez, and I. B. Mekhov, *Phys. Rev. Lett.* **124**, 010603 (2020).
- [37] A. Biella and M. Schiró, *Quantum* **5**, 528 (2021).
- [38] See Supplemental Material for a discussion on relevant technical details.
- [39] R. Bronson, *Matrix methods: An introduction* (Gulf Professional Publishing, 1991).
- [40] Y. Ashida, Z. Gong, and M. Ueda, *Advances in Physics* **69**, 249 (2020).
- [41] The condition, $\langle V_1^{(j_{\max})} | \hat{O} | V_1^{(j_{\max})} \rangle \neq 0$, may not be satisfied for some specific operators, such as the total magnetizations along x - and y -directions for $\hat{H}_{\text{TH}}^{\text{eff}}$ at $g = \gamma$. However, the integer family of dynamical scaling also exists in these cases, where $|S_y(t)| \propto t^{2L-1}$, $|S_x(t)| \propto t^{2L-2}$ (see Supplemental Material [38]).
- [42] R. Jördens, N. Strohmaier, K. Günter, H. Moritz, and T. Esslinger, *Nature* **455**, 204 (2008).
- [43] M. Schreiber, S. S. Hodgman, P. Bordia, H. P. Lüschen, M. H. Fischer, R. Vosk, E. Altman, U. Schneider, and I. Bloch, *Science* **349**, 842 (2015).
- [44] M. Boll, T. A. Hilker, G. Salomon, A. Omran, J. Nespolo, L. Pollet, I. Bloch, and C. Gross, *Science* **353**, 1257 (2016).
- [45] A. Mazurenko, C. S. Chiu, G. Ji, M. F. Parsons, M. Kanász-Nagy, R. Schmidt, F. Grusdt, E. Demler, D. Greif, and M. Greiner, *Nature* **545**, 462 (2017).
- [46] T. E. Lee and C.-K. Chan, *Phys. Rev. X* **4**, 041001 (2014).
- [47] I. Bloch, J. Dalibard, and W. Zwerger, *Rev. Mod. Phys.* **80**, 885 (2008).
- [48] D.-W. Zhang, Y.-Q. Zhu, Y. X. Zhao, H. Yan, and S.-L. Zhu, *Advances in Physics* **67**, 253 (2018).
- [49] F. Schäfer, T. Fukuhara, S. Sugawa, Y. Takasu, and Y. Takahashi, *Nature Reviews Physics* **2**, 411 (2020).
- [50] C. Monroe, W. C. Campbell, L.-M. Duan, Z.-X. Gong, A. V. Gorshkov, P. W. Hess, R. Islam, K. Kim, N. M. Linke, G. Pagano, P. Richerme, C. Senko, and N. Y. Yao, *Rev. Mod. Phys.* **93**, 025001 (2021).

Supplemental Material for “Measurement-induced integer families of critical dynamical scaling in quantum many-body systems”

I. MEASUREMENT PROTOCOL

The quantum many-body systems we discuss in the main text undergo measurements and post-selections after a brief period of unitary evolution (see Fig. 1). These processes are facilitated by the operator \hat{M} , which varies in form for spin (\hat{M}_S) and Fermi gases (\hat{M}_F) systems. This section elaborates on the experimental implementation of these measurement operators.

A. Single-site Measurement

We begin by discussing single-site measurement, corresponding to $|\mathcal{M}| = 1$. Without loss of generality, we consider the measurement and post-selection operator realized by $\hat{M}_{\text{Exp}} = 1 - k\hat{n}$, where \hat{n} has eigenvalues 1 and 0 for eigenstates $|1\rangle$ and $|0\rangle$ respectively. The relationship between \hat{M}_{Exp} and \hat{M}_S, \hat{M}_F will be clarified after general discussions.

Consider a general local state after unitary evolution and before measurement, which can be expressed as

$$|\psi(t)\rangle = c_1|1\rangle + c_0|0\rangle. \quad (\text{S1})$$

We couple $|1\rangle$ to an auxiliary state, $|a\rangle$, with a transition probability p (see Fig. 3a). The state after coupling is

$$c_1\sqrt{p}|a\rangle + c_1\sqrt{1-p}|1\rangle + c_0|0\rangle. \quad (\text{S2})$$

We can then design a scheme to detect whether the atom is in the auxiliary state, like the protocol using the signal of fluorescence in [46]. If the auxiliary state is detected, we discard this trajectory. The state in the remaining trajectories, in the absence of an auxiliary state under a small- p limit, takes the form,

$$\begin{aligned} |\psi(t+dt)\rangle &= c_1\left(1 - \frac{p}{2}\right)|1\rangle + c_0|0\rangle \\ &= \left(1 - \frac{p}{2}\hat{n}\right)|\psi(t)\rangle. \end{aligned} \quad (\text{S3})$$

It can be seen that the above post-selected state exactly coincides with $\hat{M}_{\text{Exp}}|\psi(t)\rangle$ under the condition $p = 2k$.

B. Many-site Measurement

To extend to many-site measurement cases, we first consider the two-site measurement case, where the measurement operator we aim to realize is $\hat{M}_{\text{Exp}} = 1 - k(\hat{n}_1 + \hat{n}_2)$. The subscript in \hat{n}_j for $j = 1, 2$ denotes the locations. Given a general initial state

$$|\psi(t)\rangle = c_{11}|11\rangle + c_{10}|10\rangle + c_{01}|01\rangle + c_{00}|00\rangle, \quad (\text{S4})$$

we locally couple the two $|1\rangle$ states to two auxiliary states $|a_1\rangle$ and $|a_2\rangle$, respectively. The state after coupling is expressed as

$$\begin{aligned} &c_{11} \left[(\sqrt{p})^2|a_1a_2\rangle + \sqrt{p}\sqrt{1-p}|a_11\rangle \right. \\ &\quad \left. + \sqrt{1-p}\sqrt{p}|1a_2\rangle + (\sqrt{1-p})^2|11\rangle \right] \\ &+ c_{10} \left[\sqrt{p}|a_10\rangle + \sqrt{1-p}|10\rangle \right] \\ &+ c_{01} \left[\sqrt{p}|0a_2\rangle + \sqrt{1-p}|01\rangle \right] \\ &+ c_{00}|00\rangle. \end{aligned} \quad (\text{S5})$$

As before, we discard all states in the presence of $|a_1\rangle$ or $|a_2\rangle$ such that the state in the trajectories with the absence of an auxiliary state under a small- p limit is given by

$$\begin{aligned} |\psi(t+dt)\rangle &= c_{11}(1-p)|11\rangle + c_{10}\left(1 - \frac{p}{2}\right)|10\rangle \\ &\quad + c_{01}\left(1 - \frac{p}{2}\right)|01\rangle + c_{00}|00\rangle \\ &= \left(1 - \frac{p}{2}\hat{n}_1 - \frac{p}{2}\hat{n}_2\right)|\psi(t)\rangle. \end{aligned} \quad (\text{S6})$$

This state exactly coincides with $\hat{M}_{\text{Exp}}|\psi(t)\rangle$ under the same condition $p = 2k$.

Therefore, the measurement protocol for many-site measurement cases with an operator $\hat{M}_{\text{Exp}} = 1 - k\sum_{j \in \mathcal{M}} \hat{n}_j$ can be straightforwardly generalized from the above two-site cases. In short, given a general initial state, we locally couple all the $|1\rangle$ states to a series of auxiliary states with a probability $p = 2k$ of transitioning to it. The relative probability of a state that does not couple to the auxiliary state is $(\sqrt{1-2k})^{\langle \sum_{j \in \mathcal{M}} \hat{n}_j \rangle}$, where $\langle \sum_{j \in \mathcal{M}} \hat{n}_j \rangle$ counts the total number of the local $|1\rangle$ states within the measurement region \mathcal{M} . After post-selection, the final state coincides with the action of \hat{M}_{Exp} on the initial state in the small- k limit.

C. Fermi Gases

For Fermi gases in deep optical lattices at half filling, the measurement operator in the small- dt limit is approximately

$$\begin{aligned} \hat{M}_F &\approx 1 - dt\gamma \sum_{j \in \mathcal{M}} 2\hat{n}_{j,\uparrow} + dt\gamma|\mathcal{M}| \\ &\approx e^{dt\gamma|\mathcal{M}|} (1 - 2dt\gamma \sum_{j \in \mathcal{M}} \hat{n}_{j,\uparrow}). \end{aligned} \quad (\text{S7})$$

For a generic state in the large- U limit, $|\psi(t)\rangle = \sum_{\{\sigma_j\}} c_{\{\sigma_j\}} |\sigma_1 \sigma_2 \cdots \sigma_L\rangle$ ($\sigma = \uparrow, \downarrow$), the state after acting the measurement operator reads

$$\begin{aligned} & \hat{M}_F |\psi(t)\rangle \\ & \approx e^{dt\gamma|\mathcal{M}|} (1 - 2dt\gamma \sum_{j \in \mathcal{M}} \hat{n}_{j,\uparrow}) |\psi(t)\rangle. \end{aligned} \quad (\text{S8})$$

This measurement operator can be realized by the above $\hat{M}_{\text{Exp}} = 1 - k \sum_{j \in \mathcal{M}} \hat{n}_j$ accompanied by a decay factor $e^{dt\gamma|\mathcal{M}|}$ once we make the following identifications

$$k = 2dt\gamma, \quad (\text{S9})$$

$$|0\rangle = |\downarrow\rangle, |1\rangle = |\uparrow\rangle, \quad (\text{S10})$$

$$\hat{n}_j = \hat{n}_{j,\uparrow}. \quad (\text{S11})$$

D. Spin Model

For the spin model, the measurement operator takes the form

$$\hat{M}_S = 1 - \gamma dt \sum_{j \in \mathcal{M}} (1 - \hat{\sigma}_j^y). \quad (\text{S12})$$

It can be realized by $\hat{M}_{\text{Exp}} = 1 - k \sum_{j \in \mathcal{M}} \hat{n}_j$ if we make the identifications,

$$k = 2dt\gamma, \quad (\text{S13})$$

$$\hat{\sigma}^y |0\rangle = +1|0\rangle, \hat{\sigma}^y |1\rangle = -1|1\rangle, \quad (\text{S14})$$

$$\hat{n}_j = (1 - \hat{\sigma}_j^y)/2. \quad (\text{S15})$$

II. FURTHER INSIGHTS INTO INTEGER FAMILIES OF DYNAMICAL SCALING

In the main text, we demonstrated that the late-time dynamics of certain observables (such as total magnetization in spin chains and total particle number in Fermi gases) exhibit power-law scaling. The exponents of this scaling linearly depend on the size of the measurement region or the lattice of the system. In this section, we provide additional numerical evidence for the integer family of dynamical scaling in transverse Ising and Heisenberg spin models. We also illustrate how the initial state influences the onset of dynamical scaling in Fermi gases in optical lattices.

A. Heisenberg chain

Figure S1 illustrates the time evolution of $|S_z(t)|$, $|S_y(t)|$, and $|S_x(t)|$ in the transverse Ising model under monitoring for different system sizes L . For $|S_z(t)|$ in Fig. S1(a), we find that the late-time dynamical scaling

can be fitted by the empirical formula $|S_z(t)| \propto t^{2L}$. Furthermore, the integer family for other observables, such as the total magnetization along other directions, suggests that the integer family of dynamical scaling takes the form t^{2L-q} for some non-negative integer q . For instance, we observe that $q = 1$ for $|S_y(t)|$ in Fig. S1(b) and $q = 2$ for $|S_x(t)|$ in Fig. S1(c).

B. Ising chain

Figure S2 illustrates the time evolution of $|S_z(t)|$, $|S_y(t)|$, and $|S_x(t)|$ in the transverse Ising model under monitoring for different sizes of measurement regions \mathcal{M} . For $|S_z(t)|$ in Fig. S2(a), we find that the late-time dynamical scaling can be fitted by the empirical formula $|S_z(t)| \propto t^{2|\mathcal{M}|}$ for $|\mathcal{M}| \leq L - 2$. Furthermore, the integer family for other observables, such as the total magnetization along other directions, suggests that the integer family of dynamical scaling takes the form $t^{2|\mathcal{M}|-q}$ within a certain valid region of \mathcal{M} for some non-negative integer q . For instance, we observe that $q = 1$ for $|S_y(t)|$ in Fig. S2(b) (valid for $|\mathcal{M}| \leq L - 2$) and $q = 0$ for $|S_x(t)|$ in Fig. S2(c) (valid for $|\mathcal{M}| \leq L - 3$).

C. Fermi gases in optical lattices

To assess the experimental complexity in this case of Fig. 3(c), we further investigate the remaining particle number N_P after postselections that is actually measured in experiments. Our analysis indicates that, after continuously discarding the experiment outputs, for system sizes $L = 2, 6, \text{ and } 10$, one needs to run about $10^1, 10^3, \text{ and } 10^4$ times of experiments to construct $N_P(t)$ in practice, respectively (see Fig. S3). This suggests that direct measurement of these scaling is indeed achievable with current experimental technology.

We also performed numerical simulations for the Fermi gases model in the large- U limit, using the initial state $|\uparrow_1, \uparrow_2, \cdots, \uparrow_L\rangle$ (Fig. S4). All other conditions were the same as those for the initial state $|\uparrow_1, \cdots, \uparrow_{L/2}, \downarrow_{L/2+1}, \cdots, \downarrow_L\rangle$ in the main text. As shown in Fig. S4(a), the late-time behaviors for the all-polarized initial state are the same as those for the half-polarized initial state, i.e., the total particle number exhibits the integer family of dynamical scaling $N(t) \propto t^{2L}$. The main difference can be seen in Fig. S4(b), which indicates that after continuously discarding the experimental outputs, for system sizes $L = 2, 6, \text{ and } 10$, one needs to run about $10^2, 10^4, \text{ and } 10^6$ times of experiments to construct $N_P(t)$ in practice, respectively.

For more general cases without a deep optical lattice, the measurement operator is

$$\hat{M}_F = 1 - dt\gamma \sum_{j \in \mathcal{M}} (\hat{n}_{j,\uparrow} - \hat{n}_{j,\downarrow}). \quad (\text{S16})$$

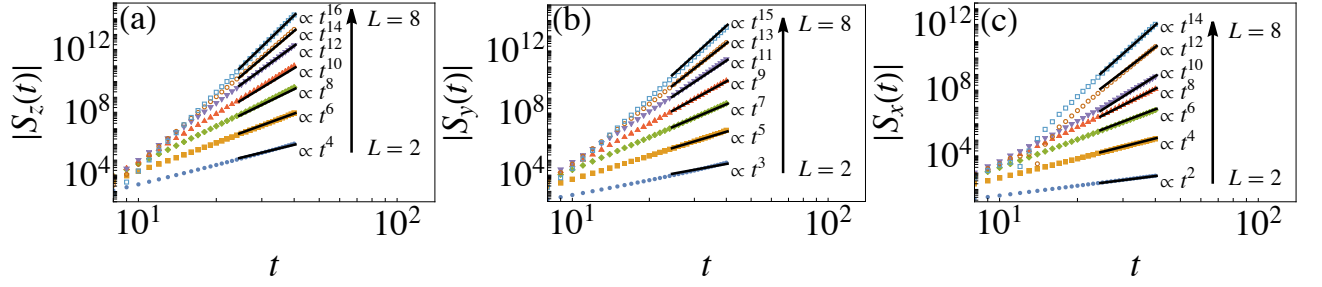


Figure S1. Quantum dynamics of the transverse Heisenberg model under monitoring. All dynamics were simulated with $J = g = \gamma = 1$, $dt = 10^{-3}$, $\mathcal{M} = \{1\}$, and the initial state given by $|\psi(t=0)\rangle = 2^{-L} \sum_{\{\sigma_i\}} |\sigma_1 \sigma_2 \cdots \sigma_L\rangle$. (a-c) Power law scaling of $|S_z(t)|$ (a), $|S_y(t)|$ (b), and $|S_x(t)|$ (c) for different system sizes. The late-time dynamics of $|S_z(t)|$ (a), $|S_y(t)|$ (b), and $|S_x(t)|$ (c) manifest the integer family of scaling $|S_z(t)| \propto t^{2L}$, $|S_y(t)| \propto t^{2L-1}$, and $|S_x(t)| \propto t^{2L-2}$, respectively. See the supplementary text for more details.

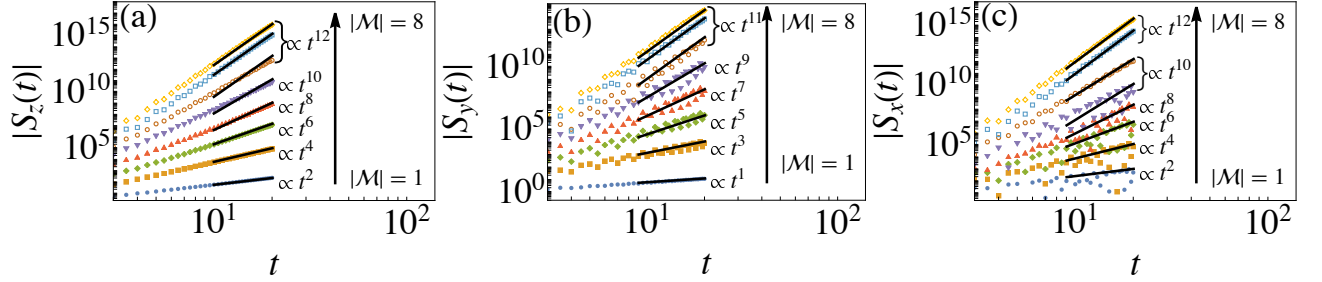


Figure S2. Quantum dynamics of the transverse Ising model under monitoring. All dynamics were simulated with $J = g = \gamma = 1$, $dt = 10^{-4}$, $L = 8$, $\mathcal{M} = \{1, 2, \dots, |\mathcal{M}|\}$, and the initial state given by $|\psi(t=0)\rangle = 2^{-L} \sum_{\{\sigma_i\}} |\sigma_1 \sigma_2 \cdots \sigma_L\rangle$. (a-c) Power law scaling of $|S_z(t)|$ (a), $|S_y(t)|$ (b), and $|S_x(t)|$ (c) for different sizes of measurement regions. The late-time dynamics of $|S_z(t)|$ (a) manifests an integer family of scaling $|S_z(t)| \propto t^{2|\mathcal{M}|}$ for $|\mathcal{M}| \leq L - 2$. The late-time dynamics of $|S_y(t)|$ (b) and $|S_x(t)|$ (c) exhibit the integer family of scaling $|S_y(t)| \propto t^{2|\mathcal{M}|-1}$ for $|\mathcal{M}| \leq L - 2$ and $|S_x(t)| \propto t^{2|\mathcal{M}|}$ for $|\mathcal{M}| \leq L - 3$, respectively. See the supplementary text for more details.

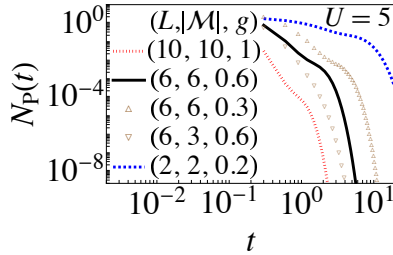


Figure S3. Time dependence of the remaining particle number N_P in Fig. 3(c) after post-selections, which is measured in experiments. The simulations were performed with $J = 1$, $dt = 10^{-3}$, and the initial state given by $|\psi(t=0)\rangle = |\uparrow_1, \dots, \uparrow_{L/2}, \downarrow_{L/2+1}, \dots, \downarrow_L\rangle$, with measurements conducted in the central region of the system. See the supplementary text for more details.

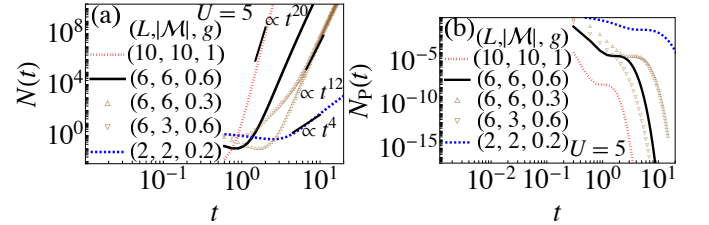


Figure S4. Quantum dynamics of Fermi gases in optical lattices under monitoring. The simulations were performed with $J = 1$, $U = 5$, $dt = 10^{-3}$, and the initial state given by $|\psi(t=0)\rangle = |\uparrow_1, \uparrow_2, \dots, \uparrow_L\rangle$, with measurements conducted in the central region of the system. (a) Power law scaling of $N(t)$ for various system and measurement region sizes exhibits an integer family of scaling $N(t) \propto t^{2L}$. (b) Time dependence of the remaining particle number N_P after post-selections, which is measured in experiments. See the supplementary text for more details.

This original form of measurement operator is more complicated than its simplified version in the large- U limit in Eq. (S7). As shown in Figs. S5(a, b), all the scaling behaviors are the same as those in the deep optical lattice, where the power law scaling $N(t) \propto t^{12}$ emerges as $\gamma/g \rightarrow 1$.

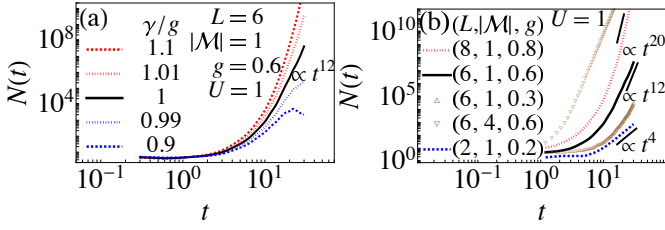


Figure S5. Quantum dynamics of Fermi gases in optical lattices under monitoring. The simulations were performed with $J = 1$, $U = 1$, $dt = 10^{-3}$, and the initial state given by $|\psi(t=0)\rangle = |\uparrow_1, \dots, \uparrow_{L/2}, \downarrow_{L/2+1}, \dots, \downarrow_L\rangle$, with measurements conducted in the central region of the system. (a) Time dependence of $N(t)$ at different γ/g for $L = 6$. Power law scaling $N(t) \propto t^{12}$ emerges as $\gamma/g \rightarrow 1$. (b) Scalings of $N(t)$ at the critical point $\gamma/g = 1$ for intermediate on-site interaction strengths. See the supplementary text for more details.

III. HIGHER ORDER EPS IN EFFECTIVE HAMILTONIANS OF MEASUREMENT DYNAMICS

Generally regarding measurements as influences imposed by the environment, the dynamics discussed in this work fall under the category of open quantum systems, typically described by the Lindblad master equation [30, 31]. However, in contrast to conventional environments where the influences are essentially random at each instant, in this scenario, the environment's effects are explicitly known through the measurement results. Consequently, this significantly simplifies the effective description of the dynamics and makes it possible to construct an effective non-Hermitian Hamiltonian [20–22] that faithfully captures the system's physics in the presence of measurements. This stands in stark contrast to the conventional open quantum systems where non-Hermitian effective Hamiltonians typically emerge as approximate descriptions to replace Lindblad master equations [40]. Here, these effective non-Hermitian Hamiltonians are instead promoted as faithful descriptions of the system's dynamics.

In the limit of continuous measurement, the effective Hamiltonians for the measurement dynamics in Ising ($\hat{H}_{\text{TI}}^{\text{eff}}$) and Heisenberg ($\hat{H}_{\text{TH}}^{\text{eff}}$) chains are found to contain the following non-Hermitian term

$$\sum_{j \in \mathcal{M}} [g\hat{\sigma}_j^x + i\gamma(1 - \hat{\sigma}_j^y)]. \quad (\text{S17})$$

Upon first inspection of this non-Hermitian term at $g = \gamma$, we discern that the local components, $\hat{\sigma}_j^x - i\hat{\sigma}_j^y$, support an EP of order two. However, the EPs of individual components do not guarantee the presence of an EP in the complete Hamiltonian. Recognizing that any arbitrary matrix can be transformed into its Jordan normal form, which is block diagonalized with the Jordan sub-block

$$J_n(\lambda) = \lambda I_n + J_n^+, \quad (\text{S18})$$

where I_n is the $n \times n$ identity matrix, and

$$J_n^+ \equiv \begin{pmatrix} 0 & 1 & 0 & \cdots & 0 & 0 \\ 0 & 0 & 1 & \cdots & 0 & 0 \\ \cdots & \cdots & \cdots & \cdots & \cdots & \cdots \\ 0 & 0 & 0 & \cdots & 0 & 1 \\ 0 & 0 & 0 & \cdots & 0 & 0 \end{pmatrix}, \quad (\text{S19})$$

we can see that if the matrix is diagonalizable, the Jordan sub-blocks have size 1, i.e., $n = 1$. For a Hamiltonian operator containing an EP of order N , its matrix representation is nondiagonalizable and thus possesses a Jordan block of size N . To ascertain the existence and the order of EPs in the effective Hamiltonian of transverse Heisenberg and Ising models under measurements, we should identify its Jordan normal form, from which the order of the EP can be directly gleaned based on the size of the Jordan sub-blocks.

A. Heisenberg Chain

1. Global Defective Term

To facilitate our discussion, we operate with the spin operators $\hat{S}^{x(y)(z)} \equiv \frac{1}{2}\hat{\sigma}^{x(y)(z)}$ ($\hbar = 1$), and redefine the energy scale J and g so that the effective Hamiltonian at $\gamma = g$ is expressed as

$$\hat{H} = -J \sum_{j=1}^{L-1} \hat{\mathbf{S}}_j \cdot \hat{\mathbf{S}}_{j+1} - g \sum_{j \in \mathcal{M}} \hat{S}_j^-, \quad (\text{S20})$$

where $\sum_{j=1}^{L-1} \hat{\mathbf{S}}_j \cdot \hat{\mathbf{S}}_{j+1} \equiv \sum_{a=x,y,z} \hat{S}_j^a \hat{S}_{j+1}^a$, $\hat{S}^\pm \equiv \hat{S}^x \pm i\hat{S}^y$, and a trivial constant $-i\gamma|\mathcal{M}|$ is disregarded. In the following, we will consider the simplest case with an open boundary condition and a global transverse field under global measurement, i.e., $\mathcal{M} = \{1, 2, \dots, L\}$.

Notice that the interaction term $-J \sum_{j=1}^{L-1} \hat{\mathbf{S}}_j \cdot \hat{\mathbf{S}}_{j+1}$ commutes with the three total spin operators ($\hat{S}^{x(y)(z)} \equiv \sum_{j=1}^L \hat{S}_j^{x(y)(z)}$). This term is invariant with respect to total spin rotation, which is the origin of saying the interaction term exhibiting a SU(2) symmetry. This symmetry has two significant implications. Firstly, the interaction term commutes with \hat{S}^2 and \hat{S}^z . As a result, the set $\{-J \sum_{j=1}^{L-1} \hat{\mathbf{S}}_j \cdot \hat{\mathbf{S}}_{j+1}, \hat{S}^2, \hat{S}^z\}$, due to the relation $[\hat{S}^2, \hat{S}^z] = 0$, shares the same eigenstates, denoted as $\{|n, s, m_s\rangle\}$. More specifically, we have

$$-J \sum_{j=1}^{L-1} \hat{\mathbf{S}}_j \cdot \hat{\mathbf{S}}_{j+1} |n, s, m_s\rangle = E_n |n, s, m_s\rangle, \quad (\text{S21})$$

$$\hat{S}^2 |n, s, m_s\rangle = (s+1)s |n, s, m_s\rangle, \quad (\text{S22})$$

$$\hat{S}^z |n, s, m_s\rangle = m_s |n, s, m_s\rangle. \quad (\text{S23})$$

Secondly, the finite rotation operator $\mathcal{D}(\hat{\mathbf{n}}, \theta) \equiv \exp(-i\hat{\mathbf{n}} \cdot \hat{\mathbf{S}}\theta)$ commutes with $-J \sum_{j=1}^{L-1} \hat{\mathbf{S}}_j \cdot \hat{\mathbf{S}}_{j+1}$. This fact highlights

the degeneracy of each eigenenergy E_n , expressed as

$$\begin{aligned} -J \sum_{j=1}^{L-1} \hat{\mathbf{S}}_j \cdot \hat{\mathbf{S}}_{j+1} (\mathcal{D}(\hat{\mathbf{n}}, \theta) |n, s, m_s\rangle) \\ = E_n (\mathcal{D}(\hat{\mathbf{n}}, \theta) |n, s, m_s\rangle). \end{aligned} \quad (\text{S24})$$

The action of $\mathcal{D}(\hat{\mathbf{n}}, \theta)$ on $|n, s, m_s\rangle$ intermixes all $|n, s, m_s\rangle$ states for $m_s = -s, \dots, s$. Therefore, each state $|n, s, m_s\rangle$ corresponds to the same energy E_n for all $m_s = -s, \dots, s$. This relationship can be understood intuitively by recognizing that the ladder operator commutes with the spin-interaction term, i.e., $[\hat{S}^\pm, -J \sum_{j=1}^{L-1} \hat{\mathbf{S}}_j \cdot \hat{\mathbf{S}}_{j+1}] = 0$. Consequently, we find that $\hat{S}^\pm |n, s, m_s\rangle = \sqrt{(s \mp m_s)(s \pm m_s + 1)} |n, s, m_s \pm 1\rangle$ possesses the same eigenenergy (E_n) as $|n, s, m_s\rangle$.

Considering the operator \hat{S}^\pm ($\equiv \sum_{j=1}^L \hat{S}_j^\pm$), it exhibits simple matrix elements within the total spin representation. Leveraging the basic properties of ladder operators, we obtain

$$\begin{aligned} \langle s', m'_{s'} | \hat{S}^\pm | s, m_s \rangle \\ = \sqrt{(s \mp m_s)(s \pm m_s + 1)} \delta_{s', s} \delta_{m'_{s'}, m_s \pm 1}, \end{aligned} \quad (\text{S25})$$

from which we infer that the matrix of \hat{S}^\pm is similar to a Jordan normal matrix, up to the factor $\sqrt{(s \mp m)(s \pm m + 1)}$. This implies that it is block-diagonalized according to different total spins and it is similar to a Jordan sub-block within each degenerate sub-space.

From the discussions above, we conclude that in the representation related to the basis $\{|n, s_n, m_s\rangle\}$ (where s_n denotes the value of s in state $|n\rangle$), the spin interaction term $-J \sum_{j=1}^{L-1} \hat{\mathbf{S}}_j \cdot \hat{\mathbf{S}}_{j+1}$ takes the form

$$\bigoplus_{n=0}^{n_{\max}} E_n I_{2s_n+1} = \begin{pmatrix} \ddots & & & & \\ & \overbrace{\begin{pmatrix} E_n & 0 & 0 & \cdots & 0 \\ 0 & E_n & 0 & \cdots & \vdots \\ \vdots & 0 & \ddots & \cdots & \vdots \\ 0 & \cdots & 0 & E_n & 0 \\ 0 & \cdots & \cdots & 0 & E_n \end{pmatrix}}^{(2s_n+1) \times (2s_n+1)} & & & \\ & & \ddots & & \end{pmatrix} \quad (\text{S26})$$

and the defective part, $-g\hat{S}^-$, takes the form

$$\bigoplus_{n=0}^{n_{\max}} \mathbb{J}_{2s_n+1} = \begin{pmatrix} \ddots & & & & \\ & \overbrace{\begin{pmatrix} 0 & -g\sqrt{2s} & \cdots & 0 \\ \vdots & 0 & \ddots & \vdots \\ 0 & \cdots & 0 & -g\sqrt{2s} \\ 0 & \cdots & 0 & 0 \end{pmatrix}}^{(2s_n+1) \times (2s_n+1)} & & & \\ & & \ddots & & \end{pmatrix} \quad (\text{S27})$$

Therefore, the matrix representation of the complete Hamiltonian \hat{H} is given by

$$H = \bigoplus_{n=0}^{n_{\max}} (E_n I_{2s_n+1} + \mathbb{J}_{2s_n+1}). \quad (\text{S28})$$

Without loss of generality, we can order E_n such that E_0 is the lowest energy and $E_{n \neq 0} - E_0 \neq 0$. The rank of $H - E_0 I_{2L}$ can be shown to be

$$\text{rank}(H - E_0 I_{2L}) = 2^L - 1. \quad (\text{S29})$$

Given that \mathbb{J}_{2s_n+1} is a nilpotent matrix satisfying $(\mathbb{J}_{2s_n+1})^{2s_n+1} = \mathbf{0}_{2s_n+1}$, we can further deduce that

$$\text{rank}((H - E_0 I_{2L})^p) = \begin{cases} 2s_n + 1 - p, & p \leq 2s_0 + 1 \\ 0 & p > 2s_0 + 1 \end{cases}. \quad (\text{S30})$$

Provided the invertible matrix S transforms H to its Jordan normal form, denoted as $S^{-1}HS = J_H$, we find

$$S^{-1}(H - E_0 I_{2L})^p S = (J_H - \bigoplus_{n=0}^{n_{\max}} E_n I_{2s_n+1})^p, \quad (\text{S31})$$

which yields

$$\begin{aligned} \text{rank} \left((J_H - \bigoplus_{n=0}^{n_{\max}} E_n I_{2s_n+1})^p \right) \\ = \text{rank}((H - E_0 I_{2L})^p) \\ = \begin{cases} 2s_n + 1 - p, & p \leq 2s_0 + 1 \\ 0 & p > 2s_0 + 1 \end{cases}. \end{aligned} \quad (\text{S32})$$

The unique ansatz of the Jordan normal matrix satisfying the above relation reads

$$J_H = J'_H \oplus J_{2s_0+1}(E_0), \quad (\text{S33})$$

where J' is the sub-block of the remainder. This result implies that the effective Hamiltonian has an EP of order $2s_0 + 1$ as given by the Jordan block $J_{2s_0+1}(E_0)$. In the case of a finite size L spin-1/2 system, s_0 corresponding to the ground state of the spin- $\frac{1}{2}$ Heisenberg XXX chain

depends on the system size, i.e., $s_0 = L/2$, leading to an EP of order $L + 1$.

For the Heisenberg spin chain under the periodic boundary condition, as shown in the main text, an additional index is needed to label the eigenvalue of the translation operator. However, in the ground state $|n = 0\rangle$, the translation operator assumes only one eigenvalue, since $|n = 0\rangle$ inherently satisfies translation invariance. As a result, the periodic boundary condition does not change the EP of the highest order found in the open boundary condition.

2. Arbitrary Local-Site Defective Term

Next, we discuss the case where the symmetry-breaking term and the measurement are applied simultaneously to those local sites in \mathcal{M} . Here, the defective term, $-g \sum_{j \in \mathcal{M}} \hat{S}_j^-$, cannot be expressed using total spin

operators. It can, however, be expressed as the partial spin operator $-g \hat{S}_1^-$, with $\hat{S}_1^{x(y)(z)} \equiv \sum_{j \in \mathcal{M}} \hat{S}_j^{x(y)(z)}$. Furthermore, we introduce the partial spin operator for the remaining part, $\hat{S}_2^{x(y)(z)} \equiv \sum_{j \notin \mathcal{M}} \hat{S}_j^{x(y)(z)}$. Thus, the defective term, $-g \hat{S}_1^-$, can be fully expressed as

$$-g \hat{S}_1^- \otimes \hat{I}_2. \quad (\text{S34})$$

In the decoupled representation with respect to $\{|s_1, m_{s_1}; s_2, m_{s_2}\rangle\}$, the defective term's matrix elements are

$$\begin{aligned} & \langle s'_1, m'_{s'_1}; s'_2, m'_{s'_2} | \hat{S}_1^- \otimes \hat{I}_2 | s_1, m_{s_1}; s_2, m_{s_2} \rangle \\ & \propto \delta_{s'_1, s_1} \delta_{m'_{s'_1}, m_{s_1} - 1} \delta_{s'_2, s_2} \delta_{m'_{s'_2}, m_{s_2}}. \end{aligned} \quad (\text{S35})$$

In the coupled basis, $\{|s, m_s\rangle\}$, the matrix elements are given by

$$\begin{aligned} & \langle s', m'_{s'} | \hat{S}_1^- \otimes \hat{I}_2 | s, m_s \rangle \\ & = \sum_{\substack{s'_1, m'_{s'_1}, s'_2, m'_{s'_2} \\ s_1, m_{s_1}, s_2, m_{s_2}}} \langle s', m'_{s'} | s'_1, m'_{s'_1}; s'_2, m'_{s'_2} \rangle \langle s'_1, m'_{s'_1}; s'_2, m'_{s'_2} | \hat{S}_1^- \otimes \hat{I}_2 | s_1, m_{s_1}; s_2, m_{s_2} \rangle \langle s_1, m_{s_1}; s_2, m_{s_2} | s, m_s \rangle \\ & = \sum_{s_1, m_{s_1}, s_2, m_{s_2}} \sqrt{(s_1 + m_{s_1})(s_1 - m_{s_1} + 1)} \langle s', m'_{s'} | s_1, m_{s_1} - 1; s_2, m_{s_2} \rangle \langle s_1, m_{s_1}; s_2, m_{s_2} | s, m_s \rangle. \end{aligned} \quad (\text{S36})$$

From the basic properties of Clebsch-Gordan coefficients, we know that

$$m_s = m_{s_1} + m_{s_2}, \quad m'_{s'} = m_{s_1} - 1 + m_{s_2} \quad (\text{S37})$$

must be satisfied for each non-zero term in the above summation. This implies that $m'_{s'} = m_s - 1$ must be satisfied for non-zero matrix element of $-g \hat{S}_1^- \otimes \hat{I}_2$ in the coupled basis, yielding

$$\langle s', m'_{s'} | (-g \hat{S}_1^- \otimes \hat{I}_2) | s, m_s \rangle \propto \delta_{m'_{s'}, m_s - 1}. \quad (\text{S38})$$

Let's denote the matrix representation of $-g \hat{S}_1^- \otimes \hat{I}_2$ with respect to the basis $\{|n, s_n, m_s\rangle\}$ as $\mathbb{M}^{(1)}$. The matrix elements in row $(n', s'_{n'}, m'_{s'})$, column (n, s_n, m_s) are given by

$$\mathbb{M}^{(1)}_{(n', s'_{n'}, m'_{s'}), (n, s_n, m_s)} = C^{(1)}_{(n', s'_{n'}, m'_{s'}), (n, s_n, m_s)} \delta_{m'_{s'}, m_s - 1} \quad (\text{S39})$$

where $C^{(1)}_{(n', s'_{n'}, m'_{s'}), (n, s_n, m_s)}$ is a coefficient. Therefore the complete effective Hamiltonian has the matrix representation

$$H \equiv \bigoplus_{n=0}^{n_{\max}} E_n I_{2s_{n+1}} + \mathbb{M}^{(1)}. \quad (\text{S40})$$

From this point, we aim to demonstrate that the Jordan normal matrix of H is given by $J_{2s_0+1}(E_0) \oplus J'$, where J' denotes the sub-block corresponding to the remainder. We reorder the index such that $s_0 = \max(\{s_n\})$ for convenience in our argument. We begin by verifying that E_0 is indeed an eigenvalue of \hat{H} with respect to the eigenstate $|n = 0, s_n = s_0, m_s = -s_0\rangle$,

$$\begin{aligned} & \hat{H} |0, s_0, -s_0\rangle \\ & = \sum_{n', s'_{n'}, m'_{s'}} |n', s'_{n'}, m'_{s'}\rangle H_{(n', s'_{n'}, m'_{s'}), (0, s_0, -s_0)} \\ & = \sum_{n', s'_{n'}, m'_{s'}} |n', s'_{n'}, m'_{s'}\rangle E_{n'} \delta_{n', 0} \delta_{s'_{n'}, s_0} \delta_{m'_{s'}, -s_0} \\ & \quad + \sum_{n', s'_{n'}, m'_{s'}} |n', s'_{n'}, m'_{s'}\rangle C_{(n', s'_{n'}, m'_{s'}), (0, s_0, -s_0)} \delta_{m'_{s'}, -s_0 - 1} \\ & = E_0 |0, s_0, -s_0\rangle. \end{aligned} \quad (\text{S41})$$

The last step employs $s_0 = \max(\{s_n\})$, implying that

$\delta_{m'_s, -s_0-1}$ does not contribute to the summation. Given that each matrix can be similar to a matrix in Jordan normal form and that similarity transformation maintains the rank invariant, we can directly compute the rank of $\tilde{H} = H - \bigoplus_{n=0}^{n_{\max}} E_0 I_{2s_n+1}$ to various powers to derive the characteristics of the Jordan sub-block associated with $|n=0\rangle$. The matrix of \tilde{H} can be expressed as

$$\begin{pmatrix} \ddots & & \vdots \\ & \overbrace{\begin{pmatrix} 0 & * & 0 & \cdots & 0 \\ \vdots & \ddots & * & \ddots & \vdots \\ \cdots & 0 & \cdots & 0 & * & 0 \\ \vdots & \ddots & \vdots & \ddots & * \\ 0 & \cdots & 0 & \cdots & 0 \end{pmatrix}}^{(2s_0+1) \times (2s_0+1)} & \\ \vdots & & \vdots \end{pmatrix}, \quad (\text{S42})$$

where * represents the nonzero off-diagonal elements as defined by (S39). Due to the presence of cross block terms, deciphering the rank of the matrix \tilde{H} directly poses a challenge. Consequently, we employ some operations to reveal the rank.

Note that if B is an invertible square matrix, the rank of square matrix A satisfies

$$\text{rank}(A) = \text{rank}(AB) = \text{rank}(BA). \quad (\text{S43})$$

We consider those B of the elementary matrix such that BA represents the elementary row operations, and AB stands for the elementary column operations. In the case of \tilde{H} , all elements of row $(0, s_0, s_0)$ are zeros since no column with index $m_s = s_0+1$ exists, implying that the rank of \tilde{H} can at most be $d-1$ where $d = \sum_{n=0}^{n_{\max}} (2s_n+1) = 2L$. To verify this, we apply elementary column operations to eliminate some elements of the remaining rows of $|n=0\rangle$. For example, we use the nonzero * in column $(0, s_0, m_s = s_0, s_0-1, \dots, -s_0+1)$ to cancel all elements in row $(0, s_0, m_s - 1)$. After this operation, the matrix \tilde{H} transforms into

$$\begin{pmatrix} \ddots & & \vdots \\ & \overbrace{\begin{pmatrix} 0 & * & 0 & \cdots & 0 \\ \vdots & \ddots & * & \ddots & \vdots \\ \cdots & 0 & \cdots & 0 & * & 0 \\ \vdots & \ddots & \vdots & \ddots & * \\ 0 & \cdots & 0 & \cdots & 0 \end{pmatrix}}^{(2s_0+1) \times (2s_0+1)} & \\ \vdots & & \vdots \end{pmatrix}. \quad (\text{S44})$$

Subsequently, we can employ elementary row operations to eliminate all the elements in the upper-right block us-

ing the nonzero *'s, leading to

$$\begin{pmatrix} & & \begin{pmatrix} 0 & \cdots & 0 & \cdots & 0 \\ \vdots & \vdots & \vdots & \vdots & \vdots \\ 0 & \cdots & 0 & \cdots & 0 \\ \vdots & \vdots & \vdots & \vdots & \vdots \\ 0 & \cdots & 0 & \cdots & 0 \end{pmatrix} \\ \vdots & & \vdots \\ \begin{pmatrix} 0 & \cdots & 0 & \cdots & 0 \\ \vdots & \vdots & \vdots & \vdots & \vdots \\ 0 & \cdots & 0 & \cdots & 0 \\ \vdots & \vdots & \vdots & \vdots & \vdots \\ 0 & \cdots & 0 & \cdots & 0 \end{pmatrix} & \overbrace{\begin{pmatrix} 0 & * & 0 & \cdots & 0 \\ \vdots & \ddots & * & \ddots & \vdots \\ 0 & \cdots & 0 & * & 0 \\ \vdots & \ddots & \vdots & \ddots & * \\ 0 & \cdots & 0 & \cdots & 0 \end{pmatrix}}^{(2s_0+1) \times (2s_0+1)} \end{pmatrix}, \quad (\text{S45})$$

where the column $(0, s_0, -s_0)$ is populated with zeros since no row with $m'_s = -s_0 - 1$ exists. Importantly, the diagonal terms in the upper-left $(d - 2s_0 - 1) \times (d - 2s_0 - 1)$ block remain unaffected during the preceding elementary column operations. This can be seen as the column (n, s_n, m_s) possesses a nonzero element in row $(0, s_0, m_s - 1)$, and the * utilized to cancel it is in column $(0, s_0, m_s)$, with $\mathbb{M}_{(0, s_0, m_s), (0, s_0, m_s)}^{(1)} = 0$. Therefore, using these diagonal terms in the upper-left block to cancel all the remaining elements in the same block by either elementary row or column operations, the matrix \tilde{H} transforms into

$$\begin{pmatrix} & & \overbrace{\begin{pmatrix} 0 & * & 0 & \cdots & 0 \\ \vdots & \ddots & * & \ddots & \vdots \\ 0 & \cdots & 0 & * & 0 \\ \vdots & \ddots & \vdots & \ddots & * \\ 0 & \cdots & 0 & \cdots & 0 \end{pmatrix}}^{(2s_0+1) \times (2s_0+1)} \\ \overbrace{\begin{pmatrix} E_{n_{\max}} - E_0 & \cdots & 0 \\ \vdots & \ddots & \vdots \\ 0 & \cdots & E_1 - E_0 \end{pmatrix}}^{(d-2s_0-1) \times (d-2s_0-1)} & \oplus & \begin{pmatrix} 0 & * & 0 & \cdots & 0 \\ \vdots & \ddots & * & \ddots & \vdots \\ 0 & \cdots & 0 & * & 0 \\ \vdots & \ddots & \vdots & \ddots & * \\ 0 & \cdots & 0 & \cdots & 0 \end{pmatrix} \end{pmatrix}. \quad (\text{S46})$$

We can now determine the rank to be

$$\begin{aligned} \text{rank}(\tilde{H}) &= d - 2s_0 - 1 + 2s_0 \\ &= d - 1. \end{aligned} \quad (\text{S47})$$

To investigate the rank for $p > 1$, we define the linear mapping $f: \mathbb{C}^d \rightarrow \mathbb{C}^d$ as

$$f(\mathbf{x}) = \tilde{H}\mathbf{x}, \quad (\text{S48})$$

where

$$\mathbf{x} = \begin{pmatrix} x_{(n_{\max}, s_{n_{\max}}, -s_{n_{\max}})} \\ x_{(n_{\max}, s_{n_{\max}}, -s_{n_{\max}}+1)} \\ \vdots \\ x_{(0, s_0, s_0)} \end{pmatrix} \in \mathbb{C}^d \quad (\text{S49})$$

is a $d \times 1$ column vector, with each row element being an independent complex scalar. The rank of \tilde{H} is then given

by

$$\text{rank}(\tilde{H}) = \dim_{\mathbb{C}}(f(\mathbb{C}^d)), \quad (\text{S50})$$

where the image of f is defined by

$$f(\mathbb{C}^d) = \{f(\mathbf{x}) | \mathbf{x} \in \mathbb{C}^d\}. \quad (\text{S51})$$

For ease of argument, we express column vectors in \tilde{H} as

$$\mathbf{v}_{(n,s_n,m_s)} = \begin{pmatrix} \tilde{H}_{(n_{\max},s_{n_{\max}},-s_{n_{\max}}),(n,s_n,m_s)} \\ \tilde{H}_{(n_{\max},s_{n_{\max}},-s_{n_{\max}}+1),(n,s_n,m_s)} \\ \vdots \\ \tilde{H}_{(0,s_0,s_0),(n,s_n,m_s)} \end{pmatrix}$$

such that

$$f(\mathbb{C}^d) = \text{span} \{ \mathbf{v}_{(n_{\max},s_{n_{\max}},-s_{n_{\max}})}, \dots, \mathbf{v}_{(0,s_0,s_0)} \}. \quad (\text{S52})$$

We begin by revisiting the case of $p = 1$ to understand what the result in (S47) implies in the context of the linear mapping f . Noting that $\tilde{H}_{(n',s'_n,m'_s),(0,s_0,-s_0)} = \tilde{H}_{(0,s_0,s_0),(n,s_n,m_s)} = 0$ (due to $\delta_{m'_s, m_s - 1}$ in (S39)), we find that $f(\mathbf{x})$ neither includes $x_{(0,s_0,-s_0)}$ nor contains a nonzero value in row $(0, s_0, s_0)$, i.e.,

$$f(\mathbb{C}^d) = \text{span} \{ \mathbf{v}_{(n_{\max},s_{n_{\max}},-s_{n_{\max}})}, \dots, \mathbf{v}_{(1,s_1,s_1)}, \mathbf{v}_{(0,s_0,-s_0+1)}, \dots, \mathbf{v}_{(0,s_0,s_0)} \}, \quad (\text{S53})$$

$$f(\mathbf{x}) = \begin{pmatrix} \sum_{(n,s_n,m_s)} \tilde{H}_{(n_{\max},s_{n_{\max}},-s_{n_{\max}}),(n,s_n,m_s)} x_{(n,s_n,m_s)} \\ \vdots \\ \sum_{(n,s_n,m_s)} \tilde{H}_{(0,s_0,s_0-1),(n,s_n,m_s)} x_{(n,s_n,m_s)} \\ 0 \end{pmatrix}. \quad (\text{S54})$$

This equation implies that $f(\mathbb{C}^d)$ is spanned by $d - 1$ vectors, resulting in $\dim_{\mathbb{C}}(f(\mathbb{C}^d)) \leq d - 1$. From the result in (S47), i.e.,

$$\dim_{\mathbb{C}}(f(\mathbb{C}^d)) = d - 1, \quad (\text{S55})$$

we infer that $\mathbf{v}_{(n_{\max},s_{n_{\max}},-s_{n_{\max}})}, \mathbf{v}_{(n_{\max},s_{n_{\max}},-s_{n_{\max}}+1)}, \dots, \mathbf{v}_{(0,s_0,s_0-1)}$ form a basis for $f(\mathbb{C}^d)$, implying they are linearly independent. This also suggests that we require $d - 1$ independent complex scalars as the coordinates of the vector $f(\mathbf{x})$ within a basis. Consequently, we introduce the following compact notation,

$$\mathbf{x}^{(1)} \equiv f(\mathbf{x}) = \begin{pmatrix} x_{(n_{\max},s_{n_{\max}},-s_{n_{\max}})}^{(1)} \\ \vdots \\ x_{(0,s_0,s_0-1)}^{(1)} \\ 0 \end{pmatrix}, \quad (\text{S56})$$

where $x_{(n,s_n,m_s) \neq (0,s_0,s_0)}^{(1)} \in \mathbb{C}$. Therefore, we find that the $d - 1$ complex scalars in $\mathbf{x}^{(1)}$ must be independent and can be regarded as the starting point for the subsequent steps.

Before generalizing to the case of an arbitrary p , let us consider $p = 2$ and examine how the structure of $f(\mathbf{x})$ is extended to $f(f(\mathbb{C}^d))$. Observing that $f(f(\mathbb{C}^d)) \subseteq f(\mathbb{C}^d)$ ($f(\mathbb{C}^d) \subseteq \mathbb{C}^d$), and considering that there are only $d - 1$ independent complex scalars in $\mathbf{x}^{(1)}$, we conclude that $f(\mathbf{x}^{(1)})$ does not contain $x_{(0,s_0,-s_0)}^{(1)}$ and $x_{(0,s_0,s_0)}^{(1)}$, i.e.,

$$f(f(\mathbb{C}^d)) = \text{span} \{ \mathbf{v}_{(n_{\max},s_{n_{\max}},-s_{n_{\max}})}, \dots, \mathbf{v}_{(1,s_1,s_1)}, \mathbf{v}_{(0,s_0,-s_0+1)}, \dots, \mathbf{v}_{(0,s_0,s_0-1)} \}, \quad (\text{S57})$$

$$f(\mathbf{x}^{(1)}) = \begin{pmatrix} \sum_{(n,s_n,m_s)} \tilde{H}_{(n_{\max},s_{n_{\max}},-s_{n_{\max}}),(n,s_n,m_s)} x_{(n,s_n,m_s)}^{(1)} \\ \vdots \\ \sum_{(n,s_n,m_s)} \tilde{H}_{(0,s_0,s_0-1),(n,s_n,m_s)} x_{(n,s_n,m_s)}^{(1)} \\ 0 \end{pmatrix}. \quad (\text{S58})$$

Given that the above $d - 2$ vectors are combinations of the basis vectors of $f(\mathbb{C}^d)$, they must be linearly independent and hence form the basis of $f(f(\mathbb{C}^d))$, which implies

$$\dim_{\mathbb{C}}(f(f(\mathbb{C}^d))) = d - 2. \quad (\text{S59})$$

This indicates that only $d - 2$ complex scalars are needed to characterize the vector $f(\mathbf{x}^{(1)})$. It is important to note that the sole difference between $\mathbf{x}^{(1)}$ and \mathbf{x} is the element in row $(0, s_0, s_0)$. Moreover, only row $(n', s'_n, m'_s = s_0 - 1)$ is nonzero in column $(0, s_0, s_0)$ of \tilde{H} . These observations suggest that only the rows $(n', s'_n, m'_s = s_0 - 1)$ of $f(\mathbf{x}^{(1)})$ differ from those of $f(\mathbf{x})$. From the fact that the $(d - 2s_0 - 1) \times (d - 2s_0 - 1)$ sub-block of \tilde{H} has full rank (owing to the presence of the nonzero diagonal terms), we infer that the complex scalars in rows $(n' \neq 0, s'_n, m'_s)$ of $f(\mathbf{x}^{(1)})$ are independent. As a result, the row $(0, s_0, s_0 - 1)$ of $f(\mathbf{x}^{(1)})$ must depend on other rows. To succinctly express this, we introduce the following compact notation,

$$\mathbf{x}^{(2)} \equiv f(\mathbf{x}^{(1)}) = \begin{pmatrix} x_{(n_{\max},s_{n_{\max}},-s_{n_{\max}})}^{(2)} \\ \vdots \\ x_{(0,s_0,s_0-2)}^{(2)} \\ \sum_{\substack{\{(n' \neq 0, s'_n, m'_s)\} \\ \cup \{(0, s_0, m'_s < s_0 - 1)\}}} c_{(n',s'_n,m'_s)}^{(2)} x_{(n',s'_n,m'_s)}^{(2)} \\ 0 \end{pmatrix}. \quad (\text{S60})$$

Here, the $d - 2$ complex scalars in $\mathbf{x}^{(2)}$ are independent and can be regarded as the starting point for the next step.

For $2 < p < 2s_0 + 2$, the vector in $f(\overbrace{f(\dots f(\mathbb{C}^d) \dots)}^{p-1})$ reads

$$\mathbf{x}^{(p-1)} = \begin{pmatrix} x_{(n_{\max}, s_{n_{\max}}, -s_{n_{\max}})}^{(p-1)} \\ \vdots \\ x_{(0, s_0, s_0 - (p-1))}^{(p-1)} \\ \sum_{\{(n' \neq 0, s_{n'}, m'_{s'}\}} c_{(n', s'_{n'}, m'_{s'})}^{(p-1), p-1} x_{(n', s'_{n'}, m'_{s'})}^{(p-1)} \\ \cup \{(0, s_0, m'_{s'} < s_0 - p + 1)\} \\ \vdots \\ \sum_{\{(n' \neq 0, s_{n'}, m'_{s'}\}} c_{(n', s'_{n'}, m'_{s'})}^{(2), p-1} x_{(n', s'_{n'}, m'_{s'})}^{(p-1)} \\ \cup \{(0, s_0, m'_{s'} < s_0 - p + 1)\} \\ 0 \end{pmatrix}. \quad (\text{S61})$$

Observing that $f(\overbrace{f(\dots f(\mathbb{C}^d) \dots)}^p) \subseteq \overbrace{f(f(\dots f(\mathbb{C}^d) \dots))}^{p-1}$, and considering that there are only $d - p + 1$ independent complex scalars in $\mathbf{x}^{(p-1)}$, we conclude that $f(\mathbf{x}^{(p-1)})$ does not contain $x_{(0, s_0, -s_0)}^{(p-1)}$ and $x_{(0, s_0, m'_{s'} = s_0 - (p-2), \dots, s_0)}^{(p-1)}$, i.e.,

$$\begin{aligned} & \overbrace{f(f(\dots f(\mathbb{C}^d) \dots))}^p \\ &= \text{span} \left\{ (\mathbf{v}_{(n_{\max}, s_{n_{\max}}, -s_{n_{\max}})} + *), \dots, (\mathbf{v}_{(1, s_1, s_1)} + *), \right. \\ & \quad \left. (\mathbf{v}_{(0, s_0, -s_0 + 1)} + *), \dots, (\mathbf{v}_{(0, s_0, s_0 - (p-1))} + *) \right\}. \quad (\text{S62}) \end{aligned}$$

In the above expression, different $*$'s denote different combinations of $\mathbf{v}_{(0, s_0, m'_{s'} \geq s_0 - p + 1)}$ with coefficients provided in (S61). The above $d - p$ linearly independent vectors yield

$$\dim_{\mathbb{C}}(\overbrace{f(f(\dots f(\mathbb{C}^d) \dots))}^p) = d - p. \quad (\text{S63})$$

This implies that only $d - p$ complex scalars are needed to characterize the vector $f(\mathbf{x}^{(p-1)})$. It's worth noting that the only difference between $\mathbf{x}^{(p-1)}$ and $\mathbf{x}^{(p-2)}$ is the element in row $(0, s_0, s_0 - (p - 2))$. Additionally, only row $(n', s'_{n'}, m'_{s'} = s_0 - (p - 1))$ is nonzero in column $(0, s_0, s_0 - (p - 2))$ of \tilde{H} . These observations indicate that only the rows $(n', s'_{n'}, m'_{s'} = s_0 - (p - 1))$ of $f(\mathbf{x}^{(p-1)})$ differ from those of $f(\mathbf{x}^{(p-2)})$. Given that the $(d - 2s_0 - 1) \times (d - 2s_0 - 1)$ sub-block of \tilde{H} has full rank,

we infer that the complex scalars in rows $(n' \neq 0, s'_{n'}, m'_{s'})$ of $f(\mathbf{x}^{(p-1)})$ are independent. Consequently, we deduce that the row $(0, s_0, s_0 - (p - 1))$ of $f(\mathbf{x}^{(p-1)})$ must depend on other rows. Therefore, we introduce

$$\mathbf{x}^{(p)} \equiv f(\mathbf{x}^{(p-1)}) = \begin{pmatrix} x_{(n_{\max}, s_{n_{\max}}, -s_{n_{\max}})}^{(p)} \\ \vdots \\ x_{(0, s_0, s_0 - p)}^{(p)} \\ \sum_{\{(n' \neq 0, s_{n'}, m'_{s'}\}} c_{(n', s'_{n'}, m'_{s'})}^{(p), p} x_{(n', s'_{n'}, m'_{s'})}^{(p)} \\ \cup \{(0, s_0, m'_{s'} < s_0 - p)\} \\ \vdots \\ \sum_{\{(n' \neq 0, s_{n'}, m'_{s'}\}} c_{(n', s'_{n'}, m'_{s'})}^{(2), p} x_{(n', s'_{n'}, m'_{s'})}^{(p)} \\ \cup \{(0, s_0, m'_{s'} < s_0 - p)\} \\ 0 \end{pmatrix}, \quad (\text{S64})$$

where the $d - p$ complex scalars in $\mathbf{x}^{(p)}$ are independent and can be regarded as the starting point for the next step.

For $p \geq 2s_0 + 2$, we can expect $f(\overbrace{f(\dots f(\mathbb{C}^d) \dots)}^{2s_0+2}) = \overbrace{f(f(\dots f(\mathbb{C}^d) \dots))}^{2s_0+1}$ since $\tilde{H}_{(n', s'_{n'}, m'_{s'}, (0, s_0, -s_0))} = 0$. This leads to

$$\begin{aligned} \dim_{\mathbb{C}}(\overbrace{f(f(\dots f(\mathbb{C}^d) \dots))}^{2s_0+2}) &= \dim_{\mathbb{C}}(\overbrace{f(f(\dots f(\mathbb{C}^d) \dots))}^{2s_0+1}) \\ &= d - 2s_0 - 1. \quad (\text{S65}) \end{aligned}$$

Ultimately, we derive

$$\begin{aligned} \text{rank}(\tilde{H}^p) &= \dim_{\mathbb{C}}(\overbrace{f(f(\dots f(\mathbb{C}^d) \dots))}^p) \\ &= \begin{cases} d - p, & p \leq 2s_0 + 1 \\ d - 2s_0 - 1 & p > 2s_0 + 1 \end{cases}. \quad (\text{S66}) \end{aligned}$$

Provided that the invertible matrix S transforms H to its Jordan normal form, i.e., $S^{-1}HS = J_H$, we find

$$\begin{aligned} & \text{rank} \left((J_H - \bigoplus_{n=0}^{n_{\max}} E_0 I_{2s_n+1})^p \right) \\ &= \text{rank}(\tilde{H}^p) \\ &= \begin{cases} d - p, & p \leq 2s_0 + 1 \\ d - 2s_0 - 1 & p > 2s_0 + 1 \end{cases}. \quad (\text{S67}) \end{aligned}$$

The only plausible Jordan normal matrix satisfying the above relation is

$$J_H = J'_H \oplus J_{2s_0+1}(E_0), \quad (\text{S68})$$

where J'_H represents the remaining sub-block. We now find that the effective Hamiltonian possesses an EP of order $2s_0 + 1$, as implied by the Jordan block $J_{2s_0+1}(E_0)$. For a finite-sized spin-1/2 system, where L represents the size, the s_0 associated with the ground state of the Heisenberg XXX chain depends on the system size, $s_0 = L/2$. This results in an EP of order $L + 1$.

In addition, the computation detailed above can be adjusted to accommodate the periodic boundary condition. As previously noted in the discussion of the global measurement case, this adjustment involves appending one more index to label the eigenvalue of the translation operator. The crucial structure and the final result, i.e., maximum power with respect to t , remain unaltered, as the translation operator assumes only one eigenvalue in the maximally polarized state $|n = 0\rangle$.

B. Ising Chain

In order to determine the existence and order of the EPs in $\hat{H}_{\text{TI}}^{\text{eff}}$, we first analyze the eigensystem of the Ising model. For the Ising model with periodic boundary conditions, the Hamiltonian is

$$\hat{H}_I = -J \sum_{j=1}^L \hat{\sigma}_j^z \hat{\sigma}_{j+1}^z, \quad (\hat{\sigma}_{L+1}^z = \hat{\sigma}_1^z) \quad (\text{S69})$$

The set of all eigenstates is given by $\{|\sigma_1 \sigma_2 \cdots \sigma_L\rangle\}$, where $\sigma \in \{\uparrow, \downarrow\}$, and $|\uparrow_j\rangle$ ($|\downarrow_j\rangle$) is the eigenstate of $\hat{\sigma}_j^z$ with an eigenenergy of $+1$ (-1). We treat the all-spin-down polarized state, $|\downarrow_1 \downarrow_2 \cdots \downarrow_L\rangle$, as the vacuum, and for convenience, write the one-magnon states as $|\mu\rangle \equiv |\downarrow_1 \downarrow_2 \cdots \uparrow_\mu \cdots \downarrow_L\rangle$. Similarly, the n -magnon states ($L - 2 \geq n \geq 2$) are represented as

$$|\mu_1, \cdots, \mu_n\rangle \equiv |\downarrow_1 \cdots \downarrow_{\mu_1-1} \uparrow_{\mu_1} \cdots \uparrow_{\mu_n} \downarrow_{\mu_n+1} \cdots \downarrow_L\rangle. \quad (\text{S70})$$

Given that the operator for the total number of domain walls can be expressed by the Hamiltonian as $\hat{D} \equiv \frac{L}{2} + \frac{\hat{H}_I}{2J}$, we can denote the energy eigenstate by the total number of domain walls $D \equiv \langle \hat{D} \rangle$. In particular, $|D; \mu_1, \mu_2, \cdots, \mu_n\rangle$ denotes the n -magnon state that has D domain walls and the same eigenenergy $E_D = J(2D - L)$. For example, all the states $|D = 2; \mu, \mu+1, \cdots, \mu+n-1\rangle$ ($L - 2 \geq n \geq 1$, $\mu \in \{1, 2, \cdots, L\}$) share the same energy $J(4 - L)$, i.e.,

$$\begin{aligned} & \hat{H}_I |2; \mu, \mu+1, \cdots, \mu+n-1\rangle \\ &= J(4 - L) |2; \mu, \mu+1, \cdots, \mu+n-1\rangle. \end{aligned} \quad (\text{S71})$$

In the following, we will examine how the local-site defective components, $\hat{\sigma}_j^x - i\hat{\sigma}_j^y$, affect the eigensystem of \hat{H}_I .

1. Single-Site Defective Term

We first consider the effective Hamiltonian at $\gamma = g$ excluding a diagonal constant, assuming periodic boundary conditions and $L > 2$. It is given by

$$\hat{H} = \hat{H}_I - 2g \hat{S}_{\mathcal{M}}^-, \quad \hat{S}_{\mathcal{M}}^- \equiv \frac{1}{2} \sum_{j \in \mathcal{M}} (\hat{\sigma}_j^x - i\hat{\sigma}_j^y). \quad (\text{S72})$$

If the measurement is applied to a single local site, $\mathcal{M} = \{m\} \subseteq \{1, 2, \cdots, L\}$, it is found that within the subspace of \hat{H}_I spanned by $\{|2; m-1\rangle, |2; m-1, m\rangle\}$, the \hat{H} has a matrix representation given by

$$\begin{pmatrix} J(4-L) & -2g \\ 0 & J(4-L) \end{pmatrix}. \quad (\text{S73})$$

Noticing that $\{|2; m-1\rangle, |2; m-1, m\rangle\}$ is decoupled to other subspaces of \hat{H}_I , we find that the matrix representation of \hat{H} takes the block-diagonal form

$$H = H' \oplus \begin{pmatrix} J(4-L) & -2g \\ 0 & J(4-L) \end{pmatrix}, \quad (\text{S74})$$

where H' represents the remaining $(2^L - 2) \times (2^L - 2)$ matrix sub-block.

The matrix H can be further transformed to its Jordan normal form using an invertible matrix S ,

$$S^{-1}HS = J'_H \oplus J_2(J(4-L)), \quad (\text{S75})$$

where J'_H is the $(2^L - 2) \times (2^L - 2)$ sub-block of the remaining matrix. The Jordan block $J_2(J(4-L))$ signals the presence of an EP of order 2 in the effective Hamiltonian \hat{H} or $\hat{H}_{\text{TI}}^{\text{eff}}$ ($\gamma = g$).

2. Continuous Many-Site Defective Term

We now consider the case where the measurement is applied to $|\mathcal{M}|$ continuous sites, $\mathcal{M} = \{m, m+1, \cdots, m+|\mathcal{M}|-1\} \subseteq \{1, 2, \cdots, L\}$, with $L-2 \geq |\mathcal{M}| \geq 2$. Within the $|\mathcal{M}| + 1$ dimensional subspace of \hat{H}_I spanned by $\{|2; m-1\rangle, |2; m-1, m\rangle, \cdots, |2; m-1, m, \dots, m+|\mathcal{M}|-1\rangle\}$, the matrix representation of \hat{H} is as follows

$$\mathbb{J}_{|\mathcal{M}+1} = \begin{pmatrix} J(4-L) & -2g & 0 & \cdots & 0 \\ 0 & J(4-L) & -2g & \cdots & 0 \\ \vdots & \vdots & \ddots & \ddots & \vdots \\ 0 & 0 & 0 & \ddots & -2g \\ 0 & 0 & 0 & \cdots & J(4-L) \end{pmatrix}. \quad (\text{S76})$$

The defective term $\hat{S}_{\mathcal{M}}^-$ acts as a ‘‘ladder’’ operator in this degenerate subspace of \hat{H}_I . As an example, consider $L = 8$, and $\mathcal{M} = \{1, 2, 3\}$. The subspace spanned by $\{|2; 8, 1, 2, 3\rangle, |2; 8, 1, 2\rangle, |2; 8, 1\rangle, |2; 8\rangle\}$ is generated by the

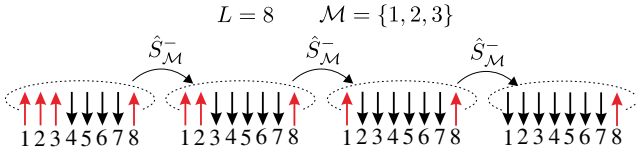


Figure S6. Symmetry for the translation of the domain wall and the effect of the defective term $\hat{S}_{\mathcal{M}}^-$. The system (S72) here is considered for $L = 8$ and $\mathcal{M} = \{1, 2, 3\}$. Four periodic boundary spin chains from the left to the right represent the states $|2; 8, 1, 2, 3\rangle$, $|2; 8, 1, 2\rangle$, $|2; 8, 1\rangle$, $|2; 8\rangle$, respectively. These states have the same number of domain wall $D = 2$, and thus the same eigenenergy $E_D = J(D - L)$ with respect to the Ising Hamiltonian \hat{H}_I . The defective term $\hat{S}_{\mathcal{M}}^-$ acts as the domain wall translation operator within this subspace.

translation of the domain wall from state $|2; 8\rangle$. As shown in Fig. S6, the defective term in the subspace transforms the states from left to right.

If the Hamiltonian contains only the matrix $\mathbb{J}_{|\mathcal{M}|+1}$, we can readily bring it to the Jordan normal form $J_{|\mathcal{M}|+1}(J(4 - L))$ and find the EP of order $|\mathcal{M}| + 1$. How-

ever, things become slightly more complicated than the case of $|\mathcal{M}| = 1$, as the aforementioned subspace will couple with other subspaces, implying that the above block is coupled with other blocks, i.e.,

$$H = \begin{pmatrix} (H') & (\text{cross terms}) \\ (\text{cross terms}) & (\mathbb{J}_{|\mathcal{M}|+1}) \end{pmatrix}, \quad (\text{S77})$$

where (H') denotes the remaining $(2^L - |\mathcal{M}| - 1) \times (2^L - |\mathcal{M}| - 1)$ matrix sub-block. While in principle we could follow the procedure outlined in the above Heisenberg case (using elementary operations and counting the dimension image space to find the rank and the Jordan normal form), the Ising model does not provide us with a concise set of indices to label the states, like n , s_n and m_s in the Heisenberg case, rendering the process tedious. As a result, we prefer to provide numerical evidence for our findings. Specifically, the effective Hamiltonian $\hat{H}_{\text{TI}}^{\text{eff}}(\gamma = g)$ with a periodic boundary condition and $L > 2$ possesses an EP of order $|\mathcal{M}| + 1$ if the measurement is applied to $|\mathcal{M}|$ continuous sites satisfying $L - 2 \geq |\mathcal{M}| \geq 1$. This results can be repeated by the following Mathematica codes [1].

These codes define the Hamiltonian:

```
H[J_,g_,L_,M_]:=Module[
{KP=KroneckerProduct, PM=PauliMatrix, KPn=Fold[KroneckerProduct][Table[#, #2]&, KPM},
KPM[a_,b_,l_,m_]:=Sum[If[l>m[[i]]>1,KP[KPn[b,m[[i]]-1],a,KPn[b,l-m[[i]]],If[m[[i]]==1,KP[a,KPn[b,l-1]],If[m[[i]]==1, KP[KPn[b,l-1],a]]],{i,Length[m]}];
-J*(KPM[KP[PM[3],PM[3]],PM[4],L-1,Range[L-1]]+KP[PM[3],KPn[PM[4],L-2],PM[3]])-g*KPM[PM[1]-I*PM[2],PM[4],L,M];
```

These codes count the order of EPs:

```
EPsOrder:=Module[{tmp=Reverse[SortBy[SplitBy[Total[JordanDecomposition[H[J,g,L,M]]][2]]/.{J->0},{2}],1,Last]}],Table[If[Total[tmp[[i]]]>0,Total[tmp[[i]]+1,0],{i,Length[tmp]}]/. {x_>,0.}:>{x}];
```

These codes provide numerical evidences for our results:

```
Do[L=i;M=Range[1,j];Print["L=",i," \[ScriptCapitalM]=",j," Order of EPs: ",OEP=EPsOrder,"-
-----Satisfy EP(\[ScriptCapitalM]+1) for \[ScriptCapitalM]<=L-2, EP(L-1) for
\[ScriptCapitalM]>L-2? ",If[j<=i-2,OEP[[1]]==j+1,OEP[[1]]==i-1]],{i,Range[3,7]},{j,Range[1,i]}];
```

IV. GENERALIZED EIGENVECTORS AND DYNAMICAL SCALING

At the exceptional point (EP), the non-Hermitian Hamiltonian becomes non-diagonalizable, leading to the coalescence of two or more energy eigenstates. This phenomenon can be observed by tracking the asymptotic behaviors of distinct eigenstates near the EP. The coalescence of eigenvectors implies a reduction in the dimension of the Hilbert space of the non-Hermitian Hamiltonian operator at the EP. However, despite this reduction, state vectors may still retain information about these lost

dimensions. Consequently, the dynamical evolution of states generated by the non-diagonalizable Hamiltonian appears unusual, as the eigenstates are insufficient to expand this state. To address this issue, we can construct generalized eigenvectors. The introduction of these vectors allows us to build a set of linearly independent basis vectors to expand any states. In the following sections, we will review the concept of generalized eigenvectors as presented in [39], derive the evolution equation given in the main text (Eq. (4)), and use it to derive the integer family of dynamical scaling in Ising and Heisenberg systems under monitoring.

A. Generalized Eigenvectors

The concept of generalized eigenvectors and their primary properties are encapsulated in the following two definitions and three theorems [39].

Definition 1. A vector $|V_n\rangle$ is a generalized eigenvector of rank n corresponding to Hamiltonian \hat{H} and eigenvalue λ if $(\hat{H} - \lambda\hat{I})^n|V_n\rangle = 0$ but $(\hat{H} - \lambda\hat{I})^{n-1}|V_n\rangle \neq 0$, where \hat{I} is the identity operator.

Note that the rank-1 generalized eigenvector is the usual eigenvector.

Definition 2. The chain generated by $|V_n\rangle$ is the set of vectors $\{|V_n\rangle, |V_{n-1}\rangle, \dots, |V_1\rangle\}$ given by the sequence

$$\begin{aligned} |V_n\rangle &= (\hat{H} - \lambda\hat{I})^{-1}|V_{n-1}\rangle = (\hat{H} - \lambda\hat{I})^{-2}|V_{n-2}\rangle \\ &= \dots = (\hat{H} - \lambda\hat{I})^{1-n}|V_1\rangle, \end{aligned} \quad (\text{S78})$$

where $|V_m\rangle$, ($m = 1, 2, \dots, n-1$) are by definition m -rank generalized eigenvectors corresponding to Hamiltonian \hat{H} and eigenvalue λ .

Theorem 1. $|V_m\rangle$ is a generalized eigenvector of rank m corresponding to Hamiltonian \hat{H} and eigenvalue λ .

Theorem 2. A chain is a linearly independent set of vectors.

Theorem 3. Every $n \times n$ matrix possesses n linearly independent generalized eigenvectors.

Theorem 3 implies that we can always use the generalized eigenvector of a Hamiltonian at the EP to study dynamical evolutions by expanding $|\psi\rangle = \sum_m a_m |E_m\rangle + \sum_{j=1}^{N_{\text{EP}}} \sum_{n=1}^{\mathcal{O}_j} c_n^{(j)} |V_n^{(j)}\rangle$, where each term is explained in the main text. Now, let's prove the evolution equation for the generalized eigenvector of rank n given in Eq. (4). Since \hat{H} and $\lambda\hat{I}$ commute, we can write the binomial formula $(\hat{H} + \lambda\hat{I})^k = \sum_{m=0}^k C_k^m \lambda^{k-m} \hat{H}^m$, yielding

$$\hat{H}^k = \sum_{m=0}^k C_k^m \lambda^{k-m} (\hat{H} - \lambda\hat{I})^m, \quad (\text{S79})$$

where $C_k^m = \frac{k!}{m!(k-m)!}$. Multiplying by $|V_n\rangle$, we obtain

$$\begin{aligned} \hat{H}^k |V_n\rangle &= \sum_{m=0}^{n-1} \frac{1}{m!} \left(\frac{k!}{(k-m)!} \lambda^{k-m} \right) \left((\hat{H} - \lambda\hat{I})^m |V_n\rangle \right) \\ &= \sum_{m=0}^{n-1} \frac{1}{m!} \frac{d^m \lambda^k}{d\lambda^m} |V_{n-m}\rangle. \end{aligned} \quad (\text{S80})$$

Considering the polynomial function of \hat{H} , $e^{-i\hat{H}t} = \sum_{k=0}^{\infty} \frac{(-it)^k}{k!} \hat{H}^k$, we find

$$\begin{aligned} e^{-iHt} |V_n\rangle &= \sum_{m=0}^{n-1} \frac{1}{m!} \frac{d^m}{d\lambda^m} \left(\sum_{k=0}^{\infty} \frac{(-it)^k}{k!} \lambda^k \right) |V_{n-m}\rangle \\ &= \sum_{m=0}^{n-1} \frac{1}{m!} \frac{d^m}{d\lambda^m} e^{-i\lambda t} |V_{n-m}\rangle \\ &= e^{-i\lambda t} \sum_{m=0}^{n-1} \frac{(-it)^m}{m!} |V_{n-m}\rangle, \end{aligned} \quad (\text{S81})$$

which is Eq. (4). It is evident that for an EP of order n , there exists a generalized eigenvector of rank n , which carries a t^{n-1} in the dynamics. Therefore, as explained in the main text, the expectation value of generic observables $\langle \psi(t) | \hat{O} | \psi(t) \rangle$ should exhibit the dynamical scaling $\propto t^{2(\mathcal{O}_{j_{\text{max}}}-1)}$ in the late-time dynamics provided $\langle V_1^{(j_{\text{max}})} | \hat{O} | V_1^{(j_{\text{max}})} \rangle \neq 0$.

B. Dynamical Scaling in Ising and Heisenberg Models

In Sec. III, we demonstrated the existence of the EP of order $L+1$ for an arbitrary $|\mathcal{M}|$ in the effective Heisenberg model with Hamiltonian $\hat{H}_{\text{TH}}^{\text{eff}}$. Notably, the rank-1 generalized eigenvector corresponding to eigenvalue E_0 is $|\Downarrow \dots \Downarrow\rangle$, i.e., $|0, s_0, -s_0\rangle$ in Eq. (S41). Taking the expectation of the total magnetization along the z -direction, we find

$$\langle \Downarrow \dots \Downarrow | \left(\sum_{j=1}^L \frac{\hat{\sigma}_j^z}{2} \right) | \Downarrow \dots \Downarrow \rangle \neq 0, \quad (\text{S82})$$

which explains the dynamical power law scaling $t^{2L} = t^{2(L+1-1)}$ in the late-time. As for the total magnetization along the other two directions, we find

$$\langle \Downarrow \dots \Downarrow | \left(\sum_{j=1}^L \frac{\hat{\sigma}_j^x}{2} \right) | \Downarrow \dots \Downarrow \rangle = 0, \quad (\text{S83})$$

$$\langle \Downarrow \dots \Downarrow | \left(\sum_{j=1}^L \frac{\hat{\sigma}_j^y}{2} \right) | \Downarrow \dots \Downarrow \rangle = 0, \quad (\text{S84})$$

which imply that the maximal scaling exponents in their late-time dynamics depend on the generalized eigenvectors of higher ranks. Nevertheless, their scaling behaviors take the form t^{2L-q} with some positive integer q , if the maximal rank n_{max} of the generalized eigenvectors in the relevant chain grow with system size at the same rate, $n_{\text{max}} \propto L$.

In Sec. III, we also demonstrated the existence of the EP of order $|\mathcal{M}|+1$ in the effective Hamiltonian $\hat{H}_{\text{TI}}^{\text{eff}}$ with periodic boundary condition $\mathcal{M} = \{m, m+1, \dots, m+|\mathcal{M}|-1\}$ and $L-2 \geq |\mathcal{M}| \geq 1$. Notably, one of the rank-1 generalized eigenvectors corresponding to eigenvalue $J(4-L)$ is $|\Downarrow_1 \dots \Downarrow_{m-2} \Uparrow_{m-1} \Downarrow_m \dots \Downarrow_L\rangle$, in which $\sum_{j=1}^L \frac{\hat{\sigma}_j^z}{2}$ has a non-vanishing expectation value. This explains the dynamical power law scaling $t^{2|\mathcal{M}|}$ in the late-time. Similarly, the expectation values for the total magnetization along the other two directions in $|\Downarrow_1 \dots \Downarrow_{m-2} \Uparrow_{m-1} \Downarrow_m \dots \Downarrow_L\rangle$ are zeros, and thus their scaling behaviors take the form $t^{2|\mathcal{M}|-q}$ with some positive integer q , if the maximal rank n_{max} of the generalized eigenvectors in the relevant chain grow with system size at the same rate, $n_{\text{max}} \propto |\mathcal{M}|$.

V. PERTURBATION THEORY AND DIVERGING TIMESCALE

The quantum dynamics discussed in our main text can be encapsulated effectively by a non-Hermitian Hamiltonian. It is reasonable to conjecture that the diverging characteristic timescales, as depicted in Figs. 2(b1-b2), near $\gamma = g$ could be a manifestation of the energy splitting in the proximity of the exceptional point (EP). In this section, we first provide a concise review of the perturbation theory near the EP [2, 3], and then demonstrate that the diverging characteristic timescale $\tau \propto |\gamma - g|^{-1/2}$, found in the main text, can indeed be explained by the energy splitting near the EP.

A. Perturbation Theory

For simplicity, let's consider a Hamiltonian in a d -dimensional Hilbert space

$$\hat{H}(\epsilon) \equiv \hat{H}_1 + \epsilon \hat{H}_2, \quad \epsilon \in \mathbb{C}. \quad (\text{S85})$$

We assume that this Hamiltonian has only one EP of order d at $\epsilon = 0$, where all the eigenvectors coalesce and the only eigenvalue is $E(0)$. We also assume that the d eigenvalues at $\epsilon \neq 0$ are distinct, i.e., $E_k(\epsilon) \neq E_n(\epsilon)$ for $k, n \in \{1, 2, \dots, d\}$ and $k \neq n$.

Now, let's restrict ϵ to be a nonzero value in the complex plane and denote the set of eigenvalues as

$$\{E_1(\epsilon), E_2(\epsilon), \dots, E_d(\epsilon)\}, \quad (\text{S86})$$

These eigenvalues are uniquely specified through the characteristic function

$$\det(\hat{H}(\epsilon) - E_n) = 0. \quad (\text{S87})$$

Next, we move the perturbation ϵ starting from z_0 , through a circle with the center being the origin, back to z_0 again. The d eigenvalues in this process can be analytically continued. When back to the same point z_0 , the d eigenvalues must either be unchanged or undergo a cyclic permutation. Without loss of generality, we assume

$$\{E_1(\epsilon), \dots, E_p(\epsilon)\}, \quad 2 \leq p \leq d \quad (\text{S88})$$

is a cycle of period p , which means that when ϵ is moved one circle, the permutation carries E_1 into E_2, \dots, E_{p-1} into E_p , and E_p into E_1 . For a given $h \in \{1, \dots, p\}$, we find $E_h(\epsilon^p)$ is a regular, single-valued function of ϵ , which allows us to develop the Laurent series, $E_h(\epsilon^p) = \sum_{m=-\infty}^{\infty} c_m \epsilon^m$, and thus

$$E_h(\epsilon) = \sum_{m=-\infty}^{\infty} c_m \epsilon^{m/p}. \quad (\text{S89})$$

The fact that all eigenvalues converge to $E(0)$ as $\epsilon \rightarrow 0$ implies that there is no negative power of ϵ , i.e., $E_h(\epsilon) = E(0) + \sum_{m=1}^{\infty} c_m \epsilon^{m/p}$. Finally, the permutation indicates the following form

$$E_h(\epsilon) = E(0) + \sum_{m=1}^{\infty} c_m e^{2\pi i m(h-1)/p} \epsilon^{m/p}, \quad (\text{S90})$$

where $h \in \{1, \dots, p\}$.

Interestingly, there will be additional constraints for a system where $\epsilon > 0$ and $\epsilon < 0$ exhibit parity-time reversal symmetry preserving and broken phase, respectively. Specifically, $\hat{H}(\epsilon > 0)$ and $\hat{H}(\epsilon < 0)$ have complete real spectra and complex conjugated spectra, respectively. First, the period of cycle in (S88) must exhibit $p > 1$, since if $p = 1$, the energies in Eq. (S90) cannot be real and complex conjugate for $\epsilon > 0$ and $\epsilon < 0$, respectively. Second, the period p can only be 2 as the eigenvalues for $\epsilon > 0$ are all real. Therefore, for every pair of eigenvalues E_{\pm} in the period of 2, they simply satisfy

$$E_{\pm}(\epsilon) = E(0) \pm \sum_{m=1}^{\infty} c_m \epsilon^{m/2}. \quad (\text{S91})$$

Especially, for a small perturbation ϵ , the gap $\Delta_E \equiv E_+ - E_-$ is found to be

$$\Delta_E \propto \epsilon^{1/2} \quad (\text{S92})$$

with an exponent 1/2.

B. Parity-Time Reversal Symmetry Transition and the Diverging Timescale

The effective Ising and Heisenberg models have the Hamiltonians

$$\hat{H}_{\text{TI}} = -J \sum_{j=1}^L \hat{\sigma}_j^z \hat{\sigma}_{j+1}^z - \sum_{j \in \mathcal{M}} (g \hat{\sigma}_j^x - i\gamma \hat{\sigma}_j^y), \quad (\text{S93})$$

$$\hat{H}_{\text{TH}} = -J \sum_{j=1}^L \sum_{a=x,y,z} \hat{\sigma}_j^a \hat{\sigma}_{j+1}^a - \sum_{j \in \mathcal{M}} (g \hat{\sigma}_j^x - i\gamma \hat{\sigma}_j^y), \quad (\text{S94})$$

For simplicity, we have dropped a trivial constant in both effective Hamiltonians, i.e., $\hat{H}_{\text{TI}} = \hat{H}_{\text{TI}}^{\text{eff}} + i\gamma|\mathcal{M}|$ and $\hat{H}_{\text{TH}} = \hat{H}_{\text{TH}}^{\text{eff}} + i\gamma|\mathcal{M}|$. We find that the energy spectra in both systems at $\gamma < g$ ($\gamma > g$) are completely real (all complex conjugate pairs) regardless of the system sizes L and the

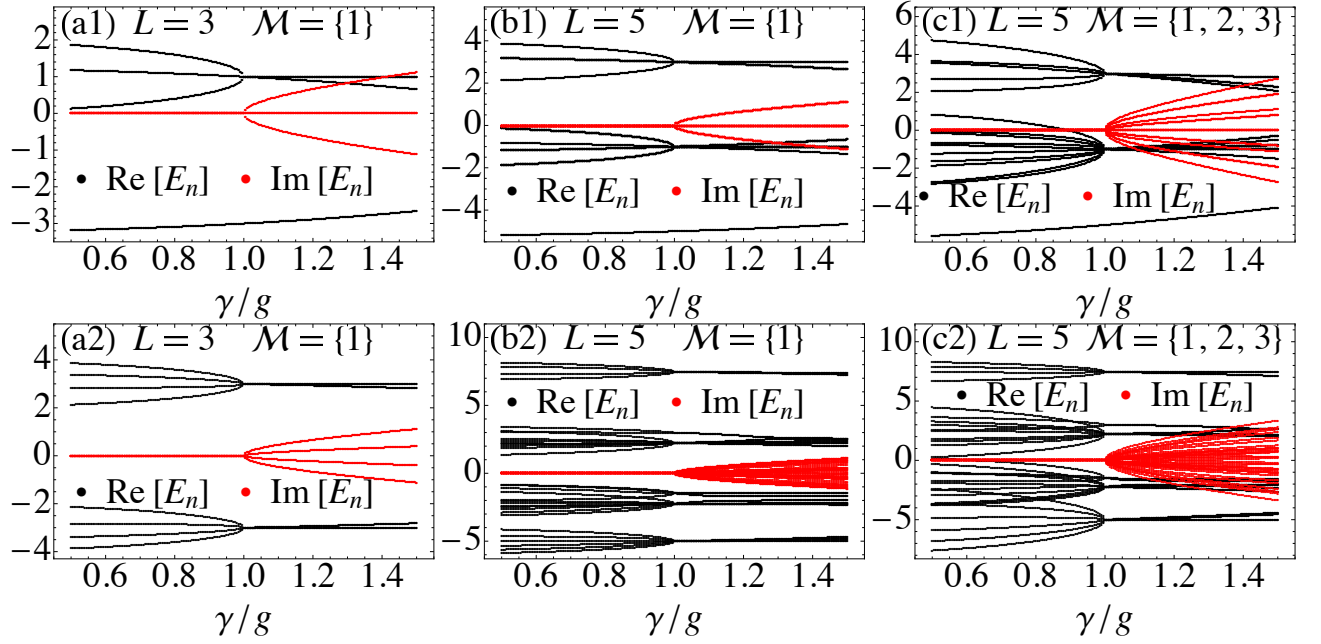


Figure S7. Spectra of effective Ising (Eq. (S93)) and Heisenberg models (Eq. (S94)). The spectra of the effective Ising model (a1-c1) and the effective Heisenberg model (a2-c2) are calculated for different system sizes ($L = 3, 5$) and measurement regions ($|\mathcal{M}| = 1, 3$ with $\mathcal{M} = \{1, 2, \dots, |\mathcal{M}|\}$). All these eigenenergies $\{E_n\}$ are completely real for $\gamma < g$ and contain complex conjugated imaginary components for $\gamma > g$.

measurement regions $|\mathcal{M}|$, as shown in Fig. S7. This indicates that the EP ($\gamma = g$) serves as the parity-time reversal symmetry transition point.

The parity-time reversal symmetry transition becomes evident if we explicit write the parity \mathcal{P} and time \mathcal{T} operators as $\mathcal{P} = \otimes_{j=1}^L \hat{\sigma}_j^y$, $\mathcal{T} = (\otimes_{j=1}^L \hat{\sigma}_j^y) \mathcal{K}$, where \mathcal{K} generates the Hermitian conjugation. The Hamiltonian \hat{H}_{TI} and \hat{H}_{TH} are \mathcal{PT} symmetric, i.e., $\mathcal{PT} \hat{H} (\mathcal{PT})^{-1} = \hat{H}$ for $\hat{H} = \hat{H}_{\text{TI}}, \hat{H}_{\text{TH}}$. The eigenstates for these Hamiltonian at $\gamma < g$ are also invariant under the action of \mathcal{PT} , while at $\gamma > g$ changes to their Hermitian conjugation. This means that the parity-time reversal symmetries of these systems are spontaneously broken at $\gamma > g$.

Both the effective Ising and Heisenberg Hamiltonians have 2^L eigenenergies in the vicinities of $\gamma = g$, denoted as $\{E_{n,1}\} \cup \{E_{n,\pm}\}$, where $E_{n,1}$ does not involve a permutation (period $p = 1$ in (S88)) and $E_{n,\pm}$ involve a permutation ($p = 2$) as discussed above. Consider a general state expanded as

$$|\psi\rangle = \sum_n c_{n,1} |E_{n,1}\rangle + \sum_n (c_{n,+} |E_{n,+}\rangle + c_{n,-} |E_{n,-}\rangle). \quad (\text{S95})$$

The dynamics of the expectation value for an arbitrary operator that is non-diagonal in the energy representation is given by $\langle \psi | e^{it\hat{H}} \hat{O} e^{-it\hat{H}} | \psi \rangle$, where the slowest modes are given by coefficients like

$$e^{\pm it(E_{n,+} - E_{n,-})}. \quad (\text{S96})$$

Especially, for $-1 \ll \frac{\gamma-g}{g} < 0$, the characteristic timescale τ in the slowest mode is fitted by the oscillation function $\cos(t/\tau)$, and exhibits

$$\tau \propto 1/|E_{n,+} - E_{n,-}| \propto |\gamma - g|^{-1/2}. \quad (\text{S97})$$

For $0 < \frac{\gamma-g}{g} \ll 1$, the characteristic timescale τ in the slowest mode is fitted by the exponential function $e^{t/\tau}$, and also exhibits

$$\tau \propto 1/|E_{n,+} - E_{n,-}| \propto |\gamma - g|^{-1/2}. \quad (\text{S98})$$

* slzhu@scnu.edu.cn

† ljlang@scnu.edu.cn

‡ liang.he@scnu.edu.cn

- [1] W. R. Inc., *Mathematica online, Version 13.3*, champaign, IL, 2023.
- [2] T. Kato, *Perturbation theory for linear operators*, vol. 132 (Springer Science & Business Media, 2013).
- [3] K. Knopp, *Theory of functions, Parts I and II* (Courier Corporation, 2013).